Ocean Dynamics (2016) 66:1559–1588
DOI 10.1007/s10236-016-0997-0

Hurricane interaction with the upper ocean in the Amazon-Orinoco plume region

Yannis Androulidakis[1] · Vassiliki Kourafalou[1] · George Halliwell[2] · Matthieu Le Hénaff[2,3] · Heesook Kang[1] · Michael Mehari[3] · Robert Atlas[2]

Received: 3 February 2016 / Accepted: 14 September 2016 / Published online: 6 October 2016

Abstract The evolution of three successive hurricanes (Katia, Maria, and Ophelia) is investigated over the river plume area formed by the Amazon and Orinoco river outflows during September of 2011. The study focuses on hurricane impacts on the ocean structure and the ocean feedback influencing hurricane intensification. High-resolution (1/25° × 1/25° horizontal grid) numerical simulations of the circulation in the extended Atlantic Hurricane Region (Caribbean Sea, Gulf of Mexico, and Northwest Atlantic Ocean) were used to investigate the upper ocean response during the three hurricane-plume interaction cases. The three hurricanes revealed different evolution and intensification characteristics over an area covered by brackish surface waters. The upper ocean response to the hurricane passages over the plume affected region showed high variability due to the interaction of oceanic and atmospheric processes. The existence of a barrier layer (BL), formed by the offshore spreading of brackish waters, probably facilitated intensification of the first storm (Hurricane Katia) because the river-induced BL enhanced the resistance of the upper ocean to cooling. This effect was missing in the subsequent two hurricanes (Maria and Ophelia) as the eroded BL (due to Katia passage) allowed the upper ocean cooling to be increased. As a consequence, the amount of ocean thermal energy provided to these storms was greatly reduced, which acted to limit intensification. Numerical experiments and analyses, in tandem with observational support, lead to the conclusion that the presence of a river plume-induced BL is a strong factor in the ocean conditions influencing hurricane intensification.

Keywords Hurricane intensification · Barrier layer · Atlantic hurricane region · Amazon-Orinoco plume · HYCOM

Responsible Editor: Pierre De Mey

✉ Yannis Androulidakis
iandroul@rsmas.miami.edu

[1] Rosenstiel School of Marine and Atmospheric Sciences, University of Miami, Miami, FL, USA

[2] NOAA-AOML, Miami, FL, USA

[3] Cooperative Institute for Marine and Atmospheric Studies, University of Miami, Miami, FL, USA

1 Introduction

The Atlantic hurricane region (including the Northwest Atlantic Ocean, the Caribbean Sea, and the Gulf of Mexico; Fig. 1) exhibits substantial interannual variability of tropical cyclone (TC) activity (Goldenberg et al. 2001). The majority of the hurricanes (80 %) originating from African easterly waves occur during August to October (95 %) and are responsible for more than 70 % of all destructions caused by TCs in the USA (Landsea and Gray 1992). A large area that extends thousands of kilometers in zonal and meridional directions over the western tropical Atlantic Ocean is covered by brackish waters originated from the Amazon and Orinoco rivers (Amazon-Orinoco hereafter in the text), modifying the oceanic conditions and thus influencing the TC activity (Ffield 2007) and the general summertime Atlantic climate (Vizy and Cook 2010). The western Atlantic Hurricane Region is thus particularly suited for the study of unique ocean and TC interaction processes. The passages of three successive hurricanes (Katia, Maria, and Ophelia) during September 2011 provide a suitable sequence of varying air-sea interaction conditions. The study objective is to examine the hurricane impacts on the ocean structure over a vast river plume area and

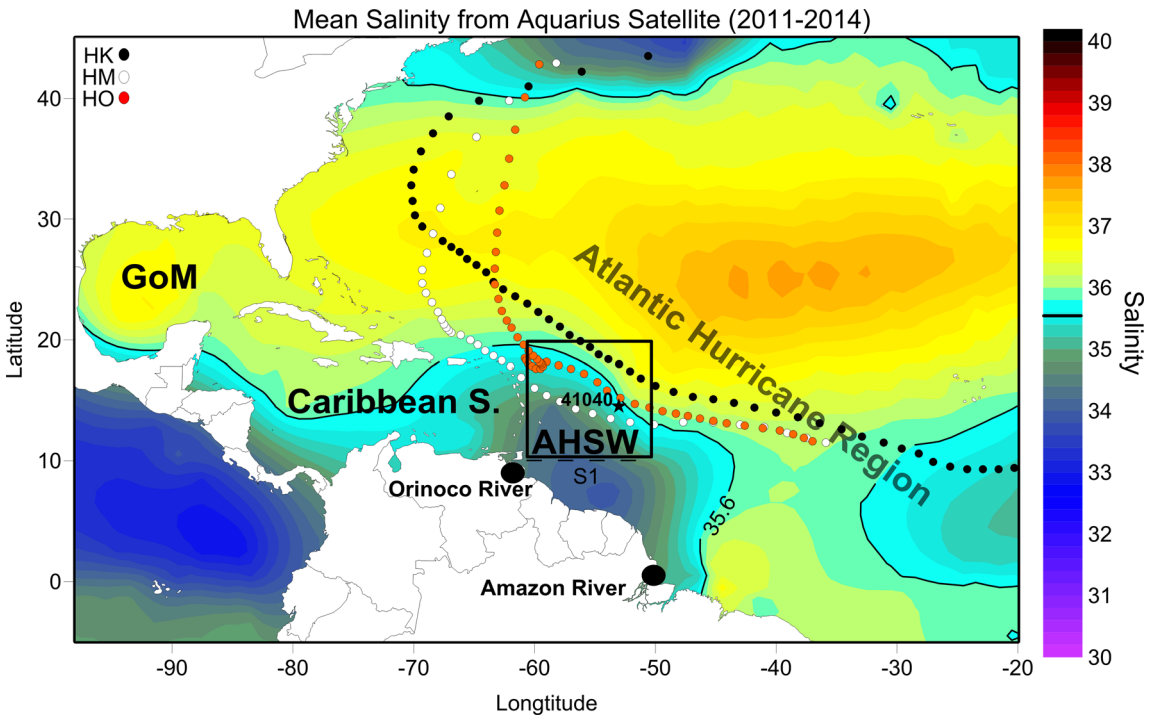

Fig. 1 Salinity distribution over the model domain, as derived and averaged from Aquarius daily observations during the period 2011–2014. The Atlantic hurricane region, Gulf of Mexico (GoM), Caribbean Sea (Caribbean S.), and Atlantic Hurricane SouthWestern (AHSW) subregions are indicated. The tracks of Hurricane Katia (HK), Hurricane Maria (HM), and Hurricane Ophelia (HO) are presented with *black*, *white*, and *red small dots*, respectively. The Orinoco and Amazon locations are also indicated with big *black dots*. The Pacific Ocean part is not included in the simulations. The location of buoy 41040 and section S1 are indicated with a *black star* and a *dashed line*, respectively

the ocean feedback, as it relates to processes affecting hurricane intensification.

The Amazon-Orinoco river system forms the largest freshwater source into the world oceans. The combined strong discharge leads to low-salinity coastal waters that spread into the equatorial Atlantic Ocean, forming an extensive buoyant plume with the lowest salinities and warmest temperatures in the region. The offshore spreading of these riverine waters is promoted by the proximity to the equator, which limits the effects of the Coriolis force. River plume dynamics dictate that the along-shelf, buoyancy-driven transport of riverine waters is due to a geostrophic balance that induces a coastal current in the direction of Kelvin-wave propagation (Kourafalou et al. 1996). Although strong for mid-latitude river plumes, this balance deteriorates for tropical plumes, the coastal current is absent and the offshore spreading of riverine waters is enhanced. This spreading is more pronounced in the summer season, aided by increased runoff and the seasonal stratification of ambient waters. Ffield (2007) showed that the brackish plume may spread over a large Atlantic region (0°—20° N, 78°–33° W) during the peak of the hurricane season (mid-August to mid-October). The brackish waters may be traced northwestward into the Caribbean Sea and northeastward into the North Atlantic (Muller-Karger et al. 1988; Muller-Karger et al. 1995; Johns et al. 1990; Coles et al. 2013). A thick low-salinity layer is observed every summer north of the Amazon-Orinoco discharge region (Masson and Delecluse 2001). Lentz (1995), based on in situ salinity measurements, showed that almost 30 % of the Amazon plume waters flow northwestward (north of 10° N) during July to October. The strong halocline, induced by the river runoff, ranges from 3 to 30 m and extends over a large part of the western tropical Atlantic Ocean during summer and fall (Pailler et al. 1999). Figure 1 showcases the extensive spreading of Amazon and Orinoco brackish waters (<35.6), as derived from Aquarius measurements and averaged during the 2011–2014 period (see Sect. 2.2).

The magnitude and fate of a TC are determined by a combination of atmospheric and oceanic conditions. Wu (2007) showed that there is strong correlation between the wetting relative humidity and the mean peak intensity of hurricanes. Other critical large-scale atmospheric processes that affect intensity involve the synoptic-scale environment (e.g., vertical wind shear, dry air entrainment, and interaction with mid-latitude troughs; Halliwell et al. 2015a). In terms of oceanic factors, Jullien et al. (2014) showed that several macro-scale dynamical processes may play a significant role on the TC intensification. There is actually a strong synergy between TC evolution and ocean response. Forced sea surface temperature (SST) cooling provides a negative feedback that can limit storm intensity by up to 50 % (Schade and Emanuel 1999). Strong currents forced by storms produce large shear at the ocean

mixed layer base, and the resulting instability of this shear layer rapidly deepens the mixed layer by up to several tens of meters in strong storms (e.g., Shay et al. 1992; Sanford et al. 2011). The resulting entrainment of deeper water typically increases the salinity and reduces the temperature of the mixed layer. Storms traveling faster than the first-mode baroclinic wave speed force a near-inertial wave train behind them, causing entrainment to persist after storm passage (Shay et al. 2000; Jullien et al. 2012). Halliwell et al. (2015a) showed that both storm size and translation speed affect hurricane intensification. They investigated the intensity evolution of large and small storms as a function of tropical cyclone heat potential (TCHP), and translation speed (their Fig. 4); for almost all storms, intensity was found substantially more sensitive to TCHP than to translation speed. The TCHP (Gray 1979) defines the ocean thermal energy and is calculated by summing the heat content in a column where the sea temperature is above 26 °C (see our Eq. 7, in Sect. 4.3, based on Leipper and Volgenau 1972). High values of TCHP have proven useful for identifying which ocean regions are favorable for hurricane intensification (Price 2009). TCHP combines the upper ocean structure and SST information into a single parameter (Mainelli et al. 2008). For high TCHP levels (e.g., river plume presence) and large TC storms, the intensity is less sensitive to translation speed.

The oceanic conditions have thus a large impact on the intensity of TC storms. When the TC moves very slowly, SST has more time to cool beneath the inner-core region, while wind-driven upwelling acts to advect colder, saltier water beneath the mixed layer toward the surface, where it can be entrained more effectively. Similarly, when the TC moves too fast, SST has little time to cool. Intense and moderately moving (<4 m s^{-1}) hurricanes cause the strongest ocean response (Price 1981), enhancing upwelling and vertical mixing. In the case of slow-moving hurricanes, small variations of translation speed may induce large variations in the mixed layer structure (Samson et al. 2009).

The above complex processes are modified in the presence of a river plume, where the associated halocline may be shallower than the thermocline. The vertical structure of the upper ocean is then divided in three layers: the upper pycnocline, determined by the salinity gradient due to the plume presence, and the barrier layer (BL) between the pycnocline and the thermocline (Masson and Delecluse 2001). Hurricane intensity is strongly related to the upper ocean properties, with intensification rates nearly 50 % higher over regions with low-salinity upper layers compared to regions without BLs (Balaguru et al. 2012a). Felton et al. (2014) employed numerical sensitivity tests to show that sea surface salinity (SSS) is the primary driver of the BL thickness (BLT) in the Indian Ocean. Similarly, the BL formed in the northwestern tropical Atlantic Ocean is sensitive to upper ocean salinity changes in the region influenced by river discharge (Balaguru et al. 2012b). In particular, the Amazon-Orinoco plume forms a strong BL (Lukas and Lindstrom 1991; Pailler et al. 1999). As a result, BLs are quasi-permanent in the equatorial and western tropical Atlantic (De Boyer Montégut et al. 2007). The stratified and stable upper ocean conditions in the presence of BLs, due to river plume spreading, may limit or prevent the intensive SST cooling that usually occurs under the hurricane's core (Wang et al. 2011; Price 1981). Haline stratification can thus play a significant role by inhibiting the surface cooling usually induced by TCs (Neetu et al. 2012) and may actually contribute to a more vigorous hurricane season (Ffield 2007). In the region influenced by the Amazon-Orinoco plume, the ocean surface cooling associated with strong storms is, indeed, reduced by 50 %, compared to surrounding open-ocean waters (Reul et al. 2014a). Storm-induced cooling and the respective negative temperature feedback are stronger over regions with thin or absent BLs (Jullien et al. 2014), promoting TC intensification. Hence, any associated changes in the BL distribution must be considered when projecting the evolution of a hurricane (Balaguru et al. 2012a).

Ffield (2007), based on historical data for the 1960–2000 period, showed that the majority of the category 5 hurricanes of the Atlantic region passed directly over the region of the Amazon-Orinoco plume. Vizy and Cook (2010) showed that the presence of the plume increases by 60 % both the number of Atlantic basin storms that form and the intensity of storms that actually form. Grodsky et al. (2012), based on new satellite salinity data, showed that Hurricane Katia (HK) left a haline wake due to mixing of the shallow BL of the Amazon-Orinoco plume over the western tropical Atlantic in early fall 2011. In addition, the presence of this shallow BL led to the warming of the SST to >29 °C, and the halocline wake was associated with at least 0.5 °C weaker SST cooling than outside the plume. Therefore, they concluded that the BL led to a reduction in hurricane-induced surface cooling that favored hurricane development. A similar effect was found in in situ measurements from a glider deployed in the southwestern Atlantic Ocean during the passage of Hurricane Gonzalo in 2014, after which the ocean recovered its prestorm vertical structure in 11 days (Domingues et al. 2015). In this study, we advance previous findings, by examining the hurricane impact on the ocean in the presence and absence of strong BL, as well as the potential ocean feedback on hurricane intensification under these varying BL conditions. In particular, we examine changes in upper ocean stratification before, during and after the HK passage (early September 2011), and their influence on the evolution of Hurricane Maria (HM) and Hurricane Ophelia (HO), which crossed the plume region a few days later (middle to late September 2011).

We use a high-resolution (0.04° × 0.04°) Hybrid Circulation Ocean Model (HYCOM) configuration, implemented over the North Atlantic Hurricane region (ATL-

HYCOM 0.04°), to perform free running simulations (*Control* run hereafter in the text) over the Atlantic hurricane region. The ATL-HYCOM 0.04° large model domain (Fig. 1) is very useful for the investigation of processes that require both high horizontal resolution (e.g., a river plume evolution) and large-scale horizontal coverage to describe efficiently the connectivity of the river plume with the broader ocean regions. The three successive hurricanes in this study formed over the eastern Atlantic hurricane region, and crossed over the South Western Atlantic Hurricane region (namely AHSW, 10° N–20° N and 50° W–60° W; Fig. 1) on September 2011. AHSW is located over the main pathway of the river plume and of many TCs, which propagate westward and toward the Caribbean Sea, the Gulf of Mexico, the eastern USA, and Canadian coasts, over the open northwestern Atlantic Ocean. Based on the National Hurricane Center's (NHC; http://www.nhc.noaa.gov) records, 88 hurricanes and tropical storms were observed during the 2009–2014 period and 24 of them formed or crossed over the AHSW region (~20 %). Most of the major Atlantic hurricanes (category 3, 4, or 5; Blake et al. 2007) pass over the Amazon-Orinoco plume area; 15 major hurricanes were detected over the Atlantic Ocean during the period 2009–2014, of which 11 passed over the AHSW subregion (>70 %), in agreement with Ffield (2007). However, the fate and evolution of these TCs were different due to specific atmospheric and upper ocean conditions. In the current study, we aim to elucidate the related processes through a case study during the 2011 hurricane season. The river plume impact on hurricane intensification and fate has been investigated in the past (e.g., Neetu et al. 2012; Grodsky et al. 2012). Recently, Balaguru et al. (2014) showed that when TCs interact with lingering cold wakes, they experience lower intensification rates. The three successive hurricane passages over the river plume region (Fig. 1), the extensive Amazon-Orinoco plume spreading, and the different hurricane characteristics consist a unique combination of different hurricane behavior with plume dynamics that allowed us to investigate the different upper ocean response during each hurricane and the differences in potential ocean feedback. We seek to explore if the riverine BL formation and erosion, and interaction between the upper ocean and the first hurricane affected the oceanic conditions during the hurricanes that followed, while also accounting for local atmospheric conditions (e.g., humidity, precipitation, storm translation speed).

The methodology, comprising of in situ observations, satellite data, model characteristics, and setup, is described in Section 2. Section 3 describes the numerical simulations and presents the major results about the performance of the model over the study area, the hurricane, and plume evolution and the distribution of the upper ocean physical characteristics. In Section 4, we discuss the hurricane-ocean interaction over the plume region. Section 5 provides a summary of concluding remarks.

2 Methods and data

2.1 The ATL-HYCOM model

The motivation of the HYCOM (https://hycom.org/) code development was to produce a real-time global and basin-scale ocean hindcast, nowcast, and prediction system in the context of the Global Ocean Data Assimilation Experiment (GODAE) (Chassignet et al. 2007). The HYCOM unique hybrid vertical discretization is an important feature that provides quasi-optimal discretization in the deep ocean (isopycnal coordinates), coastal and shelf regions (sigma and/or fixed coordinates), and the near-surface region containing the ocean mixed layer (Cartesian coordinates) (Bleck 2002 ; Halliwell 2004). The near-surface Cartesian coordinates are specified with sufficiently high vertical resolution to resolve BL structure in regions where the upper ocean is covered by low-salinity waters (Schiller et al. 2011; Androulidakis et al. 2012) such as the Amazon-Orinoco plume. Detailed information about the HYCOM model can be found in the users' manual (Bleck et al. 2002).

In this study, the simulation covers an Atlantic Ocean area from 98° W to 20° W and from 5° S to 45° N (Fig. 1). The North Atlantic grid resolution is (0.04°), and therefore, the model is called ATL-HYCOM 0.04°. This model simulation has been developed in the framework of an ocean Observing System Simulation Experiment (OSSE) system by the Ocean Modeling and OSSE Center (OMOC; http://cimas.rsmas.miami.edu/omoc.html) in Miami. The OSSE system developed by OMOC was first evaluated in the Gulf of Mexico (Halliwell et al. 2014, 2015b), and it contains a data-validated free-running model (Nature Run (NR)), a data-assimilative Forecast Model (FM), and a data assimilation toolbox that allows experiments to quantitatively evaluate specific components of any observing system. The OSSE system is a comprehensive tool for optimizing existing observing systems and designing future ones, maximizing their capability to improve model forecasts. The NR model can be further employed for process oriented studies, which are better suited in the absence of data assimilation that can mask certain dynamical aspects. This is precisely what we are doing in this study, using the NR component of the OSSE system to address the processes involved in the study objectives (*Control* run). Full OSSE experiments and observational array design are beyond the study scope. The vertical structure includes 35 hybrid layers. For the initial and boundary (through the nesting method) conditions, the global HYCOM analysis is used, which has 1/12.5° grid resolution in horizontal and 32 vertical hybrid layers (Cummings and Smedstad 2013). The bathymetry is a new 0.04° product provided by the Naval Research Laboratory (NRL; http://www.nrl.navy.mil). The ATL-HYCOM 0.04° uses the K-Profile Parameterization (KPP, described in detail in Large et al. 1994) vertical mixing

scheme with double diffusion, nonlocal boundary layer mixing and critical bulk *Ri* of 0.45.

The atmospheric forcing consists of the 3-hourly fields of precipitation, winds and surface heat flux from the US Navy NOGAPS (until 8 October 2013), replaced by NAVGEM (beginning 1 January 2013) on 0.5° grids (provided by NRL; http://www.nrl.navy.mil/), which are interpolated to the ATL-HYCOM 0.04° grid. The NOGAPS prediction system has been widely used to force ocean models that investigate oceanographic processes generated by hurricanes over the Atlantic Ocean (e.g., Zamudio and Hogan 2008). The atmospheric parameters, used in the simulations, are the precipitation (ms^{-1}), the wind speed (ms^{-1}), the vector wind stress (Nm^{-2}), the 2 m atmospheric temperature (°C), the solar and longwave radiation fluxes (Wm^{-2}), and the 2 m specific humidity (kg kg^{-1}). The relatively low resolution (0.5°) of the atmospheric model used to force our simulation is too low for resolving the small-scale features within tropical storms, in particular near the center of major storms and hurricanes. In particular, wind intensity within storms tends to be underestimated. However, the forcing we employ for this process oriented study is able to represent the large-scale changes in atmospheric conditions associated with the passages of Hurricanes Katia, Maria, and Ophelia over the Amazon-Orinoco plume area, over which these storms were not yet fully developed (see Sect. 2.4). It is thus appropriate for the related simulations and analyses.

The climatological monthly discharges of 172 rivers are included with an implementation of the estuary-like area source for the Amazon and Orinoco rivers to simulate fresh water spreading better, based on the parameterization by Schiller and Kourafalou (2010); the Amazon input is distributed over an area of about 5000 km^2. The Amazon has its maximum discharge of 261,631.2 m^3 s^{-1} in June and its minimum discharge of 116,393.4 m^3 s^{-1} in November. The Orinoco has the maximum discharge (63,382 m^3 s^{-1}) in September and the minimum discharge (6079 m^3 s^{-1}) in March. The maximum outflow summed from both rivers, occurs in July (~300,000 m^3 s^{-1}) (Barron and Smedstad 2002 and subsequent updates). The SSS values are relaxed to the monthly Generalized Digital Environmental Model (GDEM) climatology.

2.2 Satellite observations

Satellite data, covering the study region and period, were collected from three sources. The first source is the Moderate Resolution Imaging Spectroradiometer project (MODIS; http://modis.gsfc.nasa.gov/) that collects measurements of chlorophyll-a (chl-a) concentrations. The MODIS Level 3 daily products are provided by NASA's Ocean Biology Processing Group (OBPG; http://oceandata.sci.gsfc.nasa.gov/) with horizontal resolution of 4 km, covering the entire 2009–2014 study period. The collected chl-a fields are mainly used to evaluate the model simulated Amazon-Orinoco plume spreading over the Atlantic region (see Sect. 3.2).

The second source of satellite data is the Group for High Resolution SST (GHRSST; https://www.ghrsst.org/) that includes gridded surface temperature fields. SST variability is an important oceanic parameter in hurricane dynamics, affecting either the tracks of hurricanes or their intensity (Fisher 1958). However, later studies (e.g., Schade and Emanuel 1999; Kim et al. 2014) showed that the primary impact of SST is on intensity with minimal impact on track, which is primarily controlled by larger-scale atmospheric synoptic systems. The GHRSST data, used in the study, are collected from the Multi-sensor Ultra-high Resolution analysis project, which produced Level 4 SST fields with 1~2-km horizontal resolution and daily interval (Donlon et al. 2009). The Level 4 SST data were derived from the GHRSST Level 2 data by merging them objectively into a single Level 4 map. The horizontal resolution of the collected data is 1/90° × 1/90 °, covering the entire ATL-HYCOM 0.04° domain, and is used to evaluate the performance of the simulations with respect to the surface temperature during the entire simulation period (see Sect. 3.1.1).

The Aquarius project (http://aquarius.nasa.gov/) is the third group of satellite data used in the study, providing SSS estimates (Fig. 1). SSS data from the Aquarius/Satélite de Aplicaciones Científicas (SAC)-D satellite mission are provided by NASA's Jet Propulsion Laboratory (JPL) from California Institute of Technology (Lagerloef et al. 2008; Lagerloef 2012). The Aquarius Level 3 data, averaged over daily time scales, have 1° × 1° horizontal resolution and are available since 25 August 2011. According to Grodsky et al. (2012), the Aquarius data may map the Amazon-Orinoco plume with adequate precision to benefit hurricane forecasting, when it is evident that the trajectory will intersect the plume at some stage. Satellite salinity measurements derived from the Aquarius mission were used in several recent river plume studies over the Atlantic hurricane region. Grodsky et al. (2012) used Aquarius observations to elucidate the ocean and river plume evolution during HK. The year-to-year salinity changes in the Amazon plume between summer–fall of 2011 to the summer–fall of 2012 were investigated with observations from the Aquarius mission (Grodsky et al. 2014). Aquarius data were also used to document the freshening associated with the 2011 Mississippi River flooding event in the Gulf of Mexico (Gierach et al. 2013); they showed that the salinity response to this event, as observed by Aquarius, was consistent with Soil Moisture Ocean Salinity (SMOS) SSS and chl-a concentrations. Therefore, observations from the Aquarius mission can be considered sufficient to investigate the Amazon-Orinoco plume evolution and evaluate ocean simulations over the plume-influenced Atlantic hurricane region (see Sect. 3.1.1).

2.3 In situ observations

The in situ measurements used in the study are derived from the Argo system, which is a global array of more than 3000 free-drifting profiling floats that measure the temperature and salinity of the upper 2000 m of the ocean. The Argo data are publicly available in near real-time via the Global Data Assembly Centers (GDACs; http://www.argo.ucsd.edu). Every 10 days, each float collects a vertical temperature and salinity profile. The number of profiles collected over the AHSW domain during the study period (2009–2014) is approximately 2000 T/S profiles. Data from Argo floats have been widely used in model studies over the Atlantic region (e.g., Banks et al. 2012; Guinehut et al. 2002; Forget et al. 2008). Moreover, several studies about interaction between the Amazon plume and hurricanes have also included Argo float data, especially salinity measurements of the upper ocean (e.g., Grodsky et al. 2012; Grodsky et al. 2014; Reul et al. 2014b; Newinger and Toumi 2015). In situ wind and sea level pressure (SLP) measurements at buoy 41040 from the National Data Buoy Center (NDBC, http://www.ndbc.noaa.gov/), located in the center of the AHSW region (Fig. 1), were also used to study the meteorological conditions during the hurricane passages and to evaluate the atmospheric forcing fields of the ATL-HYCOM 0.04° simulation. The location of the buoy is unique for describing the hurricane characteristics, while they cross the plume-affected region.

2.4 Hurricane atmospheric data

Although atmospheric fields, derived from the NOGAPS and NAVGEM models (Sect. 2.1), were used as atmospheric forcing of the oceanic model, meteorological data contained in the National Hurricane Center (NHC, http://www.nhc.noaa.gov) "best-track" product are also used to investigate the intensity and tracks of HK (Stewart 2012), HM (Brennan 2012), and HO (Cangialosi 2011) during August, September, and October of 2011. More information about the magnitude and track of all 2009–2014 hurricanes are presented in Sect. 3.2. Sea level minimum pressure (hPa) and wind (kn) data of HK, HM, and HO hurricanes were collected every 6 h for the following periods: 28 August–7 September (HK), 6 September–15 September (HM), and 20 September–4 October (HO). The exact location of each hurricane's core is also used to investigate the hurricane track and its translation speed (ms^{-1}) over the Atlantic hurricane region. We focus on the location and intensity of the hurricane "eye," investigating the interaction between hurricanes and the upper ocean characteristics over the southwestern region of the N. Atlantic domain (AHSW; Fig. 1) during September 2011 (see Sect. 3.2). However, we note that the hurricane interaction with the ocean waters covers a much broader area (long-distance effects). Therefore, we also used the SLP from NOGAPS to compute the radius of outermost closed isobar (ROCI) for each of our study hurricanes in order to determine the storm size (see Sect. 3.2). The ROCI is defined as the average of the distances to the north, east, south, and west from the hurricane center to the closed isobar having the highest value (Merrill 1984). Three-hourly precipitation rates, derived by NOGAPS over the AHSW region, are also used to investigate the contribution of rain on the upper ocean salinity variability during the passages of hurricanes over the plume region. The respective specific humidity inside the limits of the ROCI radius along the track of each hurricane, also derived from the NOGAPS fields, is used to examine the surrounding atmospheric conditions that may influence the intensity evolution of the hurricane, especially over the study AHSW region in September 2011 (see Sect. 3.2). Figure 2a shows the good performance of NOGAPS over the AHSW region during the passages of all three hurricanes; three successive SLP drops and wind peaks (HK, HM, and HO) are observed in both measured and simulated time series in September 2011. More information about each storm's characteristics is given in Table 1.

3 Results

3.1 Model simulations and evaluation

Numerical simulations were performed with the ATL-HYCOM 0.04° model for the period 2009–2014. Two types of numerical experiments were developed: the *Control* run with realistic atmospheric, boundary and river discharge inputs, as described in Sect. 2.1, and a twin simulation, the *Noriver* run, without river discharge, in order to investigate the low-salinity plume impact on the upper ocean dynamics and its potential interaction with the TCs. All other attributes of the *Noriver* experiment are the same as in the *Control* run. We evaluated the *Control* simulation with available in situ and satellite observations, presented in Sect. 2, focusing over the hurricane-plume interaction region (AHSW; Fig. 1). A more extensive evaluation of the simulation over the whole model domain with the goal of validating it for use as the NR for the ocean OSSE system is the focus of a companion manuscript (Kourafalou et al. 2016).

3.1.1 Evaluation with satellite observations

Both GHRSST data and *Control* simulation results were averaged over the study AHSW region (Fig. 1). The cold wake of the hurricane is strongly related to substantial drops of the SST levels, under and behind the storm's "eye" (Fisher 1958). The seasonal cycle was removed from both time series in order to focus on the temperature variations due to conditions besides the seasonal cycle, such as the passage of a hurricane

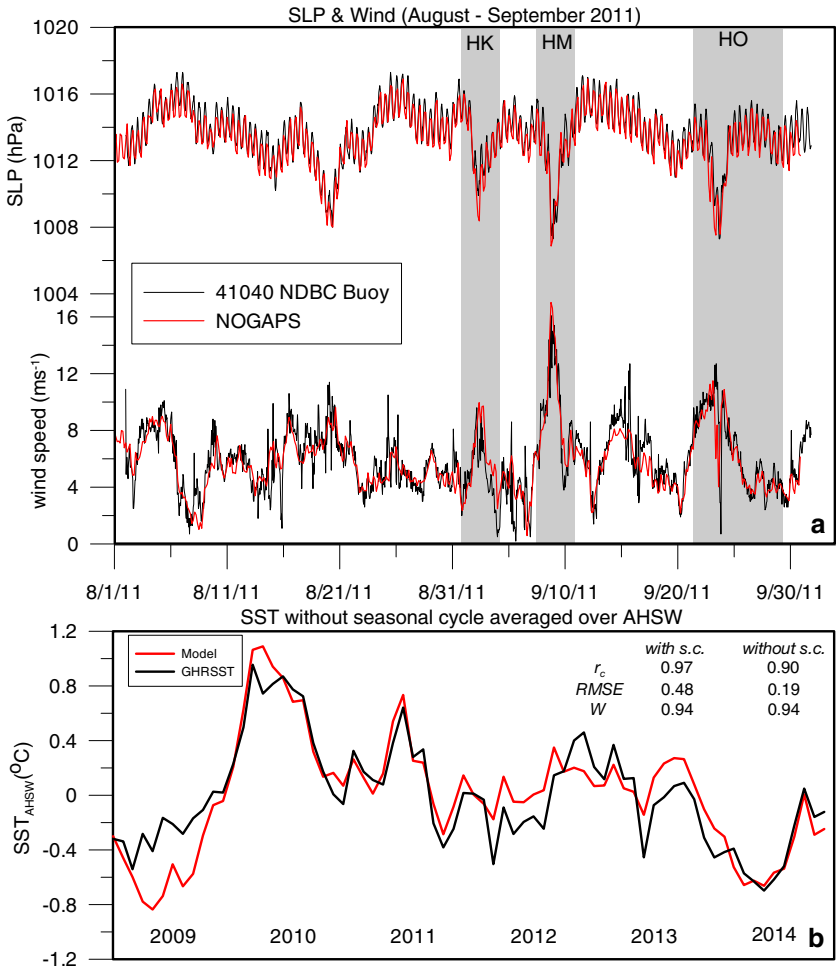

Fig. 2 **a** Evolution of sea level pressure (SLP; hPa) and wind speed (m s^{-1}) as derived from NOGAPS and observations at NDBC buoy 41040 (Fig. 1) for August–September 2011. **b** Mean monthly evolution of sea surface temperature (SST) (°C) without the seasonal cycle, averaged over the AHSW region (Fig. 1) from model and GHRSST satellite data for the period 2009–2014. The Pearson coefficient (r_c), the root mean square error (*RMSE*) and the Willmott score (*W*) for comparison with and without the seasonal cycle (s.c.) are also presented. The time period covered by each hurricane over the AHSW region is indicated with *shaded rectangles*

Table 1 Hurricanes Katia, Maria, and Ophelia major characteristics

Hurricane	Katia	Maria	Ophelia
Start date	08–28	09–06	09–20
End date	09–12	09–16	10–04
Min SLP	942/970	983/988	940/985
Max SLP (hPa NHC/NOGAPS)	1011/1008	1008/1011	1012/1010
Start location	20.3° W, 9.4° N	35.9° W, 11.5° N	37° W, 11.6° N
End location	7° W, 58° N	53.9° W, 46.7° N	31.9° W, 51.3° N
Period over AHSW	09–02	09–08	09–23
	09–04	09–10	09–28
MCP before AHSW passage	988/1001	1004/1005	997/1005
MCP after AHSW passage (hPa NHC/NOGAPS)	957/993	1005/1007	1009/1004
Wind speed before AHSW passage	65/40	45/20	50/37
Wind speed after AHSW passage (knots NHC/NOGAPS)	90/50	45/19	50/31
Translation speed before AHSW passage	8.7/9.8	10.1/10.2	5.1/4.9
Translation speed after AHSW passage (ms^{-1} NHC/NOGAPS)	5.3/6.9	7.1/7.2	2/5

or the appearance of a strong cold meteorological front. The mean monthly evolutions of both model and GHRSST data without the seasonal cycle are presented in Fig. 2b.

The simulated mean monthly evolution of SST agrees with the respective averaged measured SST, showing almost identical variation during the entire simulation period (2009–2014; Fig. 2b). The Pearson correlation coefficient (Pearson 1903), computed between the simulated and modeled values with and without the seasonal cycle, are high and equal to $r_c = 0.97$ and $r_c = 0.90$, respectively. We also employed the Willmott skill score W (Willmott 1981), following the evaluation of a Columbia River plume simulation by Liu et al. (2009) and the Mississippi River plume simulation by Androulidakis and Kourafalou (2013). The calculation of W employs the mean square error (MSE):

$$MSE = (\langle m\rangle - \langle o\rangle)^2 + (S_m - S_o)^2 + 2S_m S_o(1 - r_c) \quad (1)$$

$$W = 1 - \frac{MSE}{\left\langle (|m - \langle o\rangle| + |o - \langle o\rangle|)^2 \right\rangle} \quad (2)$$

where m and o are time series of the modeled and observed variables, respectively, and $\langle\rangle$ denotes a mean; S_m and S_o are the respective standard deviations. The W skill score for the 2009–2014 period is significantly high ($W = 0.94$) for both seasonal and seasonally adjusted comparisons, indicating the good performance of the model ($W = 1$ indicates perfect agreement between predicted and measured values). The root MSE ($RMSE$) is 0.48 °C, but the simulated time series without the seasonal cycle shows less than 0.2 °C deviations from the satellite measurements over the AHSW area (Fig. 2b). The high peaks, measured by the satellite, in early 2010 (~0.8 °C) and in mid-2011 (~0.6°) are both simulated well by the model, while both model and observations show similar strong lows (e.g., in 2009 and in 2014). Especially during the period of the three successive study hurricanes, the simulated and observed mean monthly variations are in good agreement with similar low and peak values in summer–fall 2011. More GHRSST comparisons with respect to the cold wake formation during each hurricane passage over the AHSW region are presented in Sect. 3.3.1.

The comparison between the simulated (SSS_{Model}) and observed ($SSS_{Aquarius}$) data refers to the period from September 2011 to April 2014, which includes 973 daily fields (Sect. 2.2). The horizontal distribution of low-salinity values (<35.6), as derived from both Aquarius and *Control* experiment in characteristic dates during the passage of the three study hurricanes in 2011 (HK, HM, and HO), are presented in Fig. 3. In early September 2011, the brackish waters from the Amazon-Orinoco river system reached the northern limit of the AHSW region (~20° N), while a large portion of low-salinity surface waters also advected westward, toward the Caribbean Sea, as presented in both satellite and simulated fields (Fig. 3a). The salinity increase by the end of September (Fig. 3c) over the AHSW region is also evident in both simulated and observed fields. Other regions, covered with low-salinity waters, were also well reproduced by the *Control* experiment (e.g., North Atlantic, Northern Gulf of Mexico, Equatorial region). The plume evolution is further discussed in Sects. 3.2 and 3.3.

In some areas, close to the river mouths, the model overestimates salinity by 1 unit, computing less brackish surface waters than in reality. However, the comparison between satellite and simulated time series, over the AHSW region, reveals high coefficient of determination $R^2 = 0.74$ (Fig. 4). R^2 is a statistical measure (Steel and James 1960) that provides information about the goodness of fit of a model and how well the regression line approximates the real data points ($R^2 = 1$ indicates perfect agreement between two time series):

$$R^2 = \frac{\sum_{i=1}^{n} (o_i - \langle o\rangle)^2}{\sum_{i=1}^{n} (m_i - \langle o\rangle)^2} \quad (3)$$

The averaged SSS_{Model} over the AHSW region, derived from the 32 mean monthly values, is equal to 35.39 and is very close to the respective $SSS_{Aquarius}$ (35.20). The Fig. 4 scatter plot shows a generally good agreement between the simulated and modeled data for the majority of the mean monthly values of the study period (2011–2014). Although the best agreement is observed for months with weak river plume signal and high-salinity levels (e.g., January–April), months related to the study period also show strong agreement. In particular, the values in Fig. 4 for August and September, when all three studied hurricanes were observed in 2011 (Table 1), are located very close to the identity line ($x = y$). Moreover, the Pearson correlation coefficient ($r_C = 0.85$) and the Wilmott score ($W = 0.81$), derived by all 973 daily values, are both significantly high, supporting the good performance of the model over the study AHSW region. The respective $RMSE$ is small and equal to 0.41. According to Lewis and Allen (2009) and Kourafalou and Androulidakis (2013), if the differences between the observed and model salinity values at the surface are smaller than 2 units, especially over river-affected regions, the model performance can be considered satisfactory in terms of salinity. Although the slight SSS overestimation by the model, computed close to the Amazon-Orinoco river mouths, may somewhat underestimate the intensity and the effect of the associated BL, the low $RMSE$ in surface salinity is very satisfying, especially as it is supported by a large number of measurements during the evaluation period.

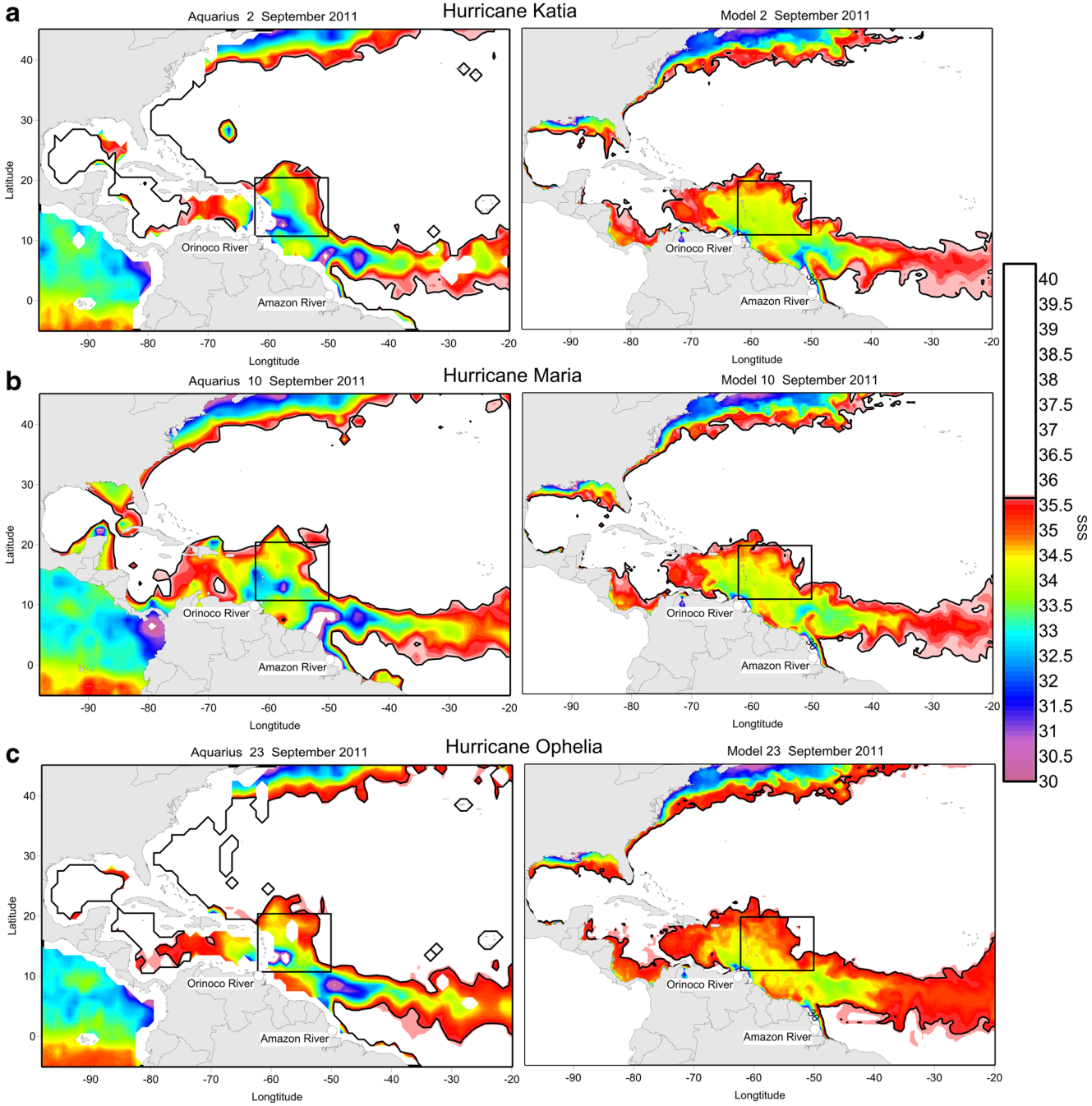

Fig. 3 Distribution of sea surface salinity (SSS) over the entire ATL-HYCOM domain from one characteristic day of **a** Hurricane Katia, **b** Hurricane Maria, and **c** Hurricane Ophelia passages over the AHSW region (*black rectangle*), as derived from Aquarius (*left panels*) and model (*right panels*) data. Values over 35.6 are excluded to highlight the low-salinity Amazon-Orinoco waters

3.1.2 Evaluation with Argo measurements

Available surface measurements, collected from the Argo floats for the entire study period from January 2009 to December 2014, are used to evaluate the simulated surface salinity and temperature of the *Control* simulation. Since Argo measurements are not available daily over the AHSW subregion during the study period, we computed the mean monthly values from both model results and in situ measurements (Fig. 5).

The seasonal variations of SST_{AHSW} and SSS_{AHSW} derived from all months of 2009–2014 are presented in Fig. 5a, c, respectively. Both measured and simulated SST levels range around 26 °C in winter and around 28 °C in early autumn, when HK, HO, and HM occurred over the study subregion (Fig. 5a); the difference of the two seasonal SST time series is overall the same for each month. Simulated and observed salinity seasonal variations, averaged for the entire study period, are also in good agreement (Fig. 5c). Low values around

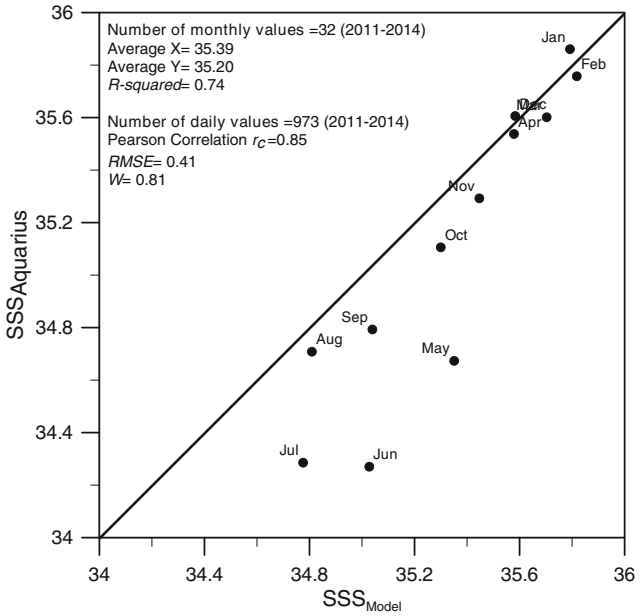

Fig. 4 Scatter diagram of sea surface salinity (SSS), averaged over all months of the 2011–2014 period and over the AHSW region (Fig. 1), as derived from daily model (SSS_{Model}) and Aquarius satellite data ($SSS_{Aquarius}$). Statistical metrics of both daily and monthly time series from September 2011 to April 2014 are also presented

35 occur in summer and early fall, when the AHSW region is usually covered with brackish river waters (Lentz 1995). On the contrary, more saline (~36) waters are observed and computed in winter. Although the model underestimates salinity levels in comparison with the Argo measurements, the maximum difference between the two seasonal time series is less than 0.5 salinity units. The *RMSE* derived from both mean monthly interannual time series is comparable (~0.5, see Fig. 5b, d). The respective *W* and r_c scores are 0.70 and 0.69 for SSS_{AHSW} and significantly high (0.95 and 0.96) for SST_{AHSW}. The salinity levels of the region are strongly affected by the spreading of the river plume and the precipitation levels during the tropical summer and fall seasons. Therefore, very low values appear during all summer months (Fig. 5d). An exception is observed in 2013, when the model simulated low-salinity waters over the AHSW region (~35), while the Argo floats measured higher levels, indicating a reduced intrusion of Amazon-Orinoco waters intrusion into the AHSW region; the climatological river forcing of the model is a possible cause of the salinity discrepancy between the model and the observations in 2013. However, the differences between the measured and modeled values are less than the estimated *RMSE* for the largest part of the period, especially during the summer and autumn seasons (<0.50; Fig. 5c). From 2009 to 2012, the differences between observed and modeled monthly SSS values are the smallest in periods of salinity minima, during the summer and autumn seasons (Fig. 5d). In particular, differences were relatively small during the 2011 time interval of the three storms studied in detail herein.

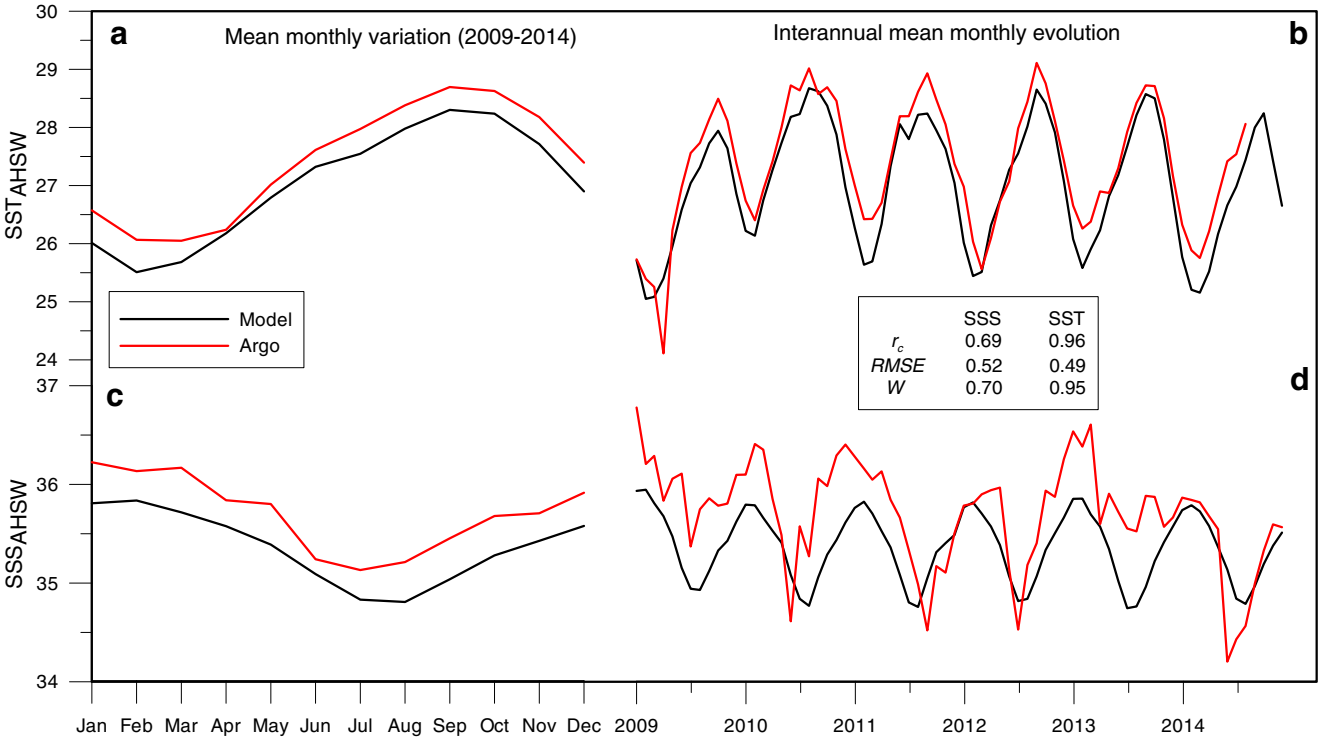

Fig. 5 Evolution of (*a*) climatological sea surface temperature (SST, °C), (*b*) mean monthly SST, (*c*) climatological sea surface salinity (SSS), and (*d*) mean monthly SSS, derived from 2009 to 2014 daily simulated and respective observed (Argo floats) values. All parameters are averaged over the AHSW region (Fig. 1)

3.2 The 2009–2014 hurricane seasons: hurricanes and plume evolution

Several TCs pass over the plume-affected study region each year (Ffield 2007) and extract their energy from the tropical ocean (Vizy and Cook 2010). During the period 2009–2014, 11 hurricanes (categories 1 to 5) crossed the AHSW region, based on NHC records). All of them formed during the August–October period and showed different evolution with respect to magnitude and track characteristics. Figure 6 shows, for all these hurricanes, the evolution of the minimum pressure in the "eye" of each hurricane (minimum central pressure (MCP)), and their wind and translation speed, collected from the NHC database. Hurricane Bill (HB) formed in mid-August 2009 and reached its maximum winds of 115 kn and its MCP of 943 hPa five days later over the AHSW region (Fig. 6a). Its translation speed remained stable over this region (~7 m s^{-1}). Hurricanes Earl (HEa) and Igor (HIg) formed off the Cape Verde islands in the end of August 2010 and early September 2010, respectively, and propagated over the AHSW region a few days later (Fig. 6b). Both of these TCs intensified before and during their passages over the AHSW; especially HIg reached Category 4, with MCP of 924 hPa and maximum winds ~135 kn on 15 September 2010. The translation speed of HIg increased a few days before its passage over AHSW and simultaneously began to intensify. It reached high translation speeds (11 m s^{-1}) 1 day before its intrusion over the plume region. A third storm, Hurricane Tomas (HT), began as tropical depression over the western Atlantic ocean in late October, close to the Amazon outflow region but started to intensify immediately, reaching in lowest MCP of 980 hPa and highest wind speed of 80 knots over the AHSW region on 31 October 2010 (Fig. 6b). Its translation speed ranges between 4 and 9 m s^{-1} during its passage over this region.

The 2011 hurricanes emphasized in the present study, HK, HM, and HO, formed at the end of August, beginning of September, and end of September 2011, respectively (Table 1; Fig. 6c). HK formed over the Cape Verde islands in the eastern Atlantic Ocean (Fig. 1), on 28 August, and entered the AHSW region on 2 September, with MCP around 988 hPa. The atmospheric pressure of the hurricane's center sharply dropped to 957 hPa during the following 2 days, while it passed over the AHSW region; the wind speed increased from 65 to 90 kn (Table 1). HK was the only one among the three successive 2011 study hurricanes that intensified during its passage over the Amazon-Orinoco plume region. Its translation speed ranged between 4 and 8 m s^{-1} over the AHSW region, which is an additional condition favoring intensification. Both HM and HO formed over the southeastern Atlantic hurricane region (Fig. 1). They showed relatively high MCP minima (>1001; Fig. 6c) during their interaction with the plume region. Balaguru et al. (2014) showed that HM, which remained "tropical storm" during its passage over the region, felt the lingering cold SST wake of HK. Moreover, although HO revealed translation speeds favorable for intensification before its intrusion over the AHSW region (~6 m s^{-1}), it weakened, showing significantly high MCPs (>1010 hPa) and low wind speed (<30 kn). Its translation speed was significantly reduced after 25 September (<3 m s^{-1}), which was an additional important factor for its even stronger attenuation (MCP peak on 25 September). Both hurricanes intensified over the central and northern Atlantic region (Fig. 1), away from the buoyant plume spreading (AHSW area). On the contrary, HK intensified over the plume, with significantly low pressure followed by strong winds. The HK winds strengthened even more (120 kn) 3 days after the storm's exit from the AHSW region (Fig. 6c). This is not the case for either HM or HO, which showed weaker and stable wind speeds during their passages over the AHSW area. Although NOGAPS atmospheric fields underestimate and overestimate the maximum wind speed and SLP, respectively, before and after the hurricane passage over the plume region, they also confirm the HK intensification and the attenuation of HM and HO over the AHSW region (Table 1; Fig. 7).

In 2012, Hurricane Ernesto (HEr) and Isaac (HIs) passed over the study plume region and slightly reduced their minimum pressure and increased their wind speed in early and late August, respectively (Fig. 6d). Their intensification over the AHSW region may also be related to their high translation speeds (~9 m s^{-1}). Although their lowest MCPs occurred later than their AHSW passages, the atmospheric pressure in the "eye" reduced over the plume area. No major TCs crossed the study area in 2013. Finally, in 2014, Hurricanes Bertha (HBe) in early August and Gonzalo (HG) in mid-October appeared over the plume affected region, revealing weak but apparent MCP reductions (Fig. 6e). It thus appears that all major TCs, except for two 2011 hurricanes (HM and HO), intensified over the plume-affected AHSW region, reducing the MCP and increasing the magnitude of the accompanying winds (e.g., HK; Table 1). The particularity of HM and HO is that they did not intensify over the AHSW, passing this area soon after HK, a storm that (on the contrary) did intensify after passing over the AHSW. The different intensification rates observed for different storms can be associated with different ocean structures and responses, but also with different atmospheric conditions, such as the translation speed.

In addition to MCP, wind and translation speed, Fig. 6 also shows the time evolution, during each hurricane, of the chl-a surface concentration, averaged over the AHSW region; we use chl-a as an indicator of the river plume spreading over the Atlantic Ocean, as it is related to waters of high nutrient content. The highest chl-a mean concentrations (>1.4 kg m^{-3}) were observed on 2 September 2011 (Fig. 6c), the first day of HK intrusion into the AHSW region, indicating the strong presence of riverine waters over the interaction region, in agreement with Aquarius and simulated SSS maps (Fig. 3). The weakening of the low-salinity signature of the plume after the HK and during

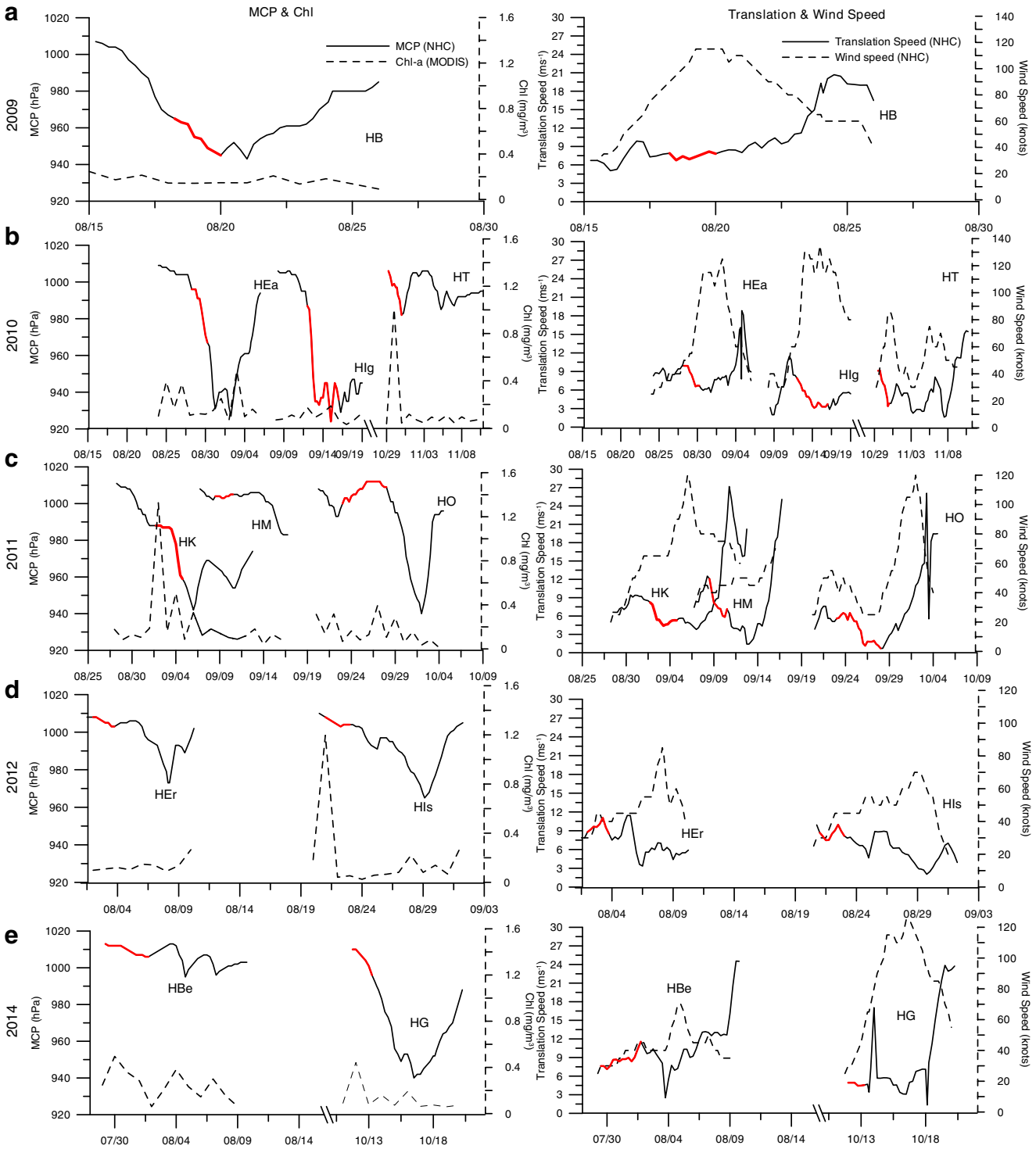

Fig. 6 Evolution of all hurricanes (tropical storms and depressions are excluded) that crossed over the AHSW region (Fig. 1) during the 2009–2014 period. *Left panels*: Measured (National Hurricane Center (NHC)) Minimum Central Pressure (MCP, in HPa, *solid line*), and the respective chlorophyll (mg m^{-3}, *dashed line*), derived from MODIS daily images and averaged over the AHSW region. *Right panels*: Measured (NHC) wind speed (kn, *dashed line*) and translation speed (m s^{-1}, *solid line*). *Red color* indicates the passage of each hurricane over the AHSW region. Hurricanes **a** Bill (HB); **b** Earl (HEa), Igor (HIg), Tomas (HT); **c** Katia (HK), Maria (HM), Ophelia (HO); **d** Ernesto (HEr), Isaac (HIs); **e** Bertha (HBe) and Gonzalo (HG) are presented. No hurricanes were observed over the AHSW region in 2013

the HM and HO passages is also indicated with respective low chl-a concentrations. The chl-a levels were gradually reduced from 1.4 to 0.4 kg m^{-3} during the HK crossing over the AHSW region and remained in low levels (<0.4 kg m^{-3}) during

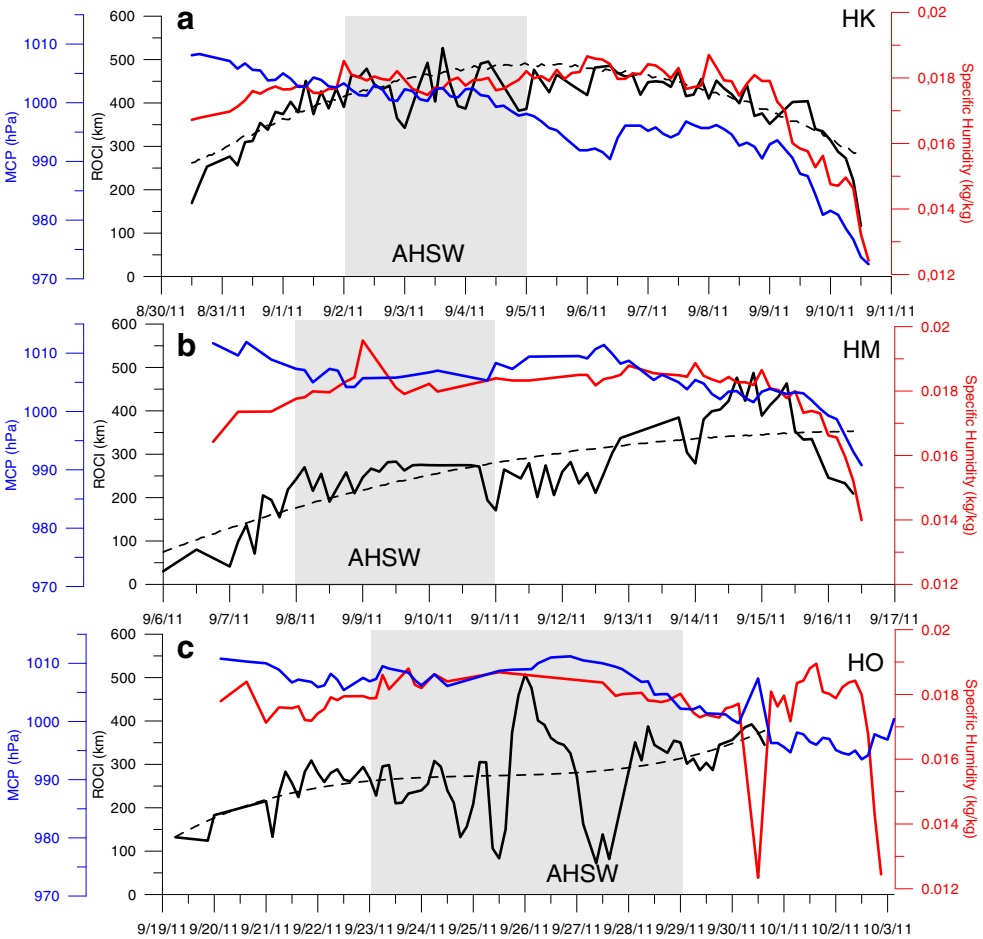

Fig. 7 Radius of outermost closest isobar (ROCI in km, *black lines*), minimum central pressure (MCP in hPa, *blue lines*), and specific humidity (kg kg^{-1}, *red lines*) evolution along the hurricane tracks for **a** Hurricane Katia (HK), **b** Hurricane Maria (HM), and **c** Hurricane Ophelia (HO), derived from NOGAPS fields. Specific humidity is averaged within the ROCI along each hurricane's track. The time period that each hurricane covered over the AHSW region (Fig. 1) is indicated with shaded rectangles. The third-degree polynomial fit for each ROCI is indicated with a *dashed black line*

both HM and HO passage. High chl-a concentrations (~1.2 kg m^{-3}) were also measured during the HT passage over the AHSW region in 2010 (Fig. 6b), when it intensified, showing its lowest MCP levels and highest wind speeds. As described above, the hurricane translation speed is also an important favorable condition for its intensification. Although HIs also passed over the plume on 2012 (as marked by the high chl-a concentrations, Fig. 6d), its intensification is weaker, probably due to the short period between formation and passage over the plume (1 day). However, none of these hurricanes was followed by another major TC. Therefore, the September 2011 period is a unique study case, with three sequential hurricanes and strong plume signal during the first one.

We note that the MCP evolution presented in Fig. 6 considers the position and magnitude of each TC at the "eye" only, although the hurricane's impact area is more extended and its effect on the upper ocean is also determined by other factors, such as the translation speed and the storm size. We thus estimated ROCI values (see definition in Sect. 2.4) for the three study hurricanes of 2011, in order to determine the size of each TC and the outermost extent of its wind circulation that may affect the upper ocean mixing (Fig. 7). The ROCI of HK reveals large values (~500 km; Fig. 7a) over the AHSW region, showing characteristics of a large storm in terms of size, in agreement with Merrill (1984), who argued that the large TC is defined as one with a ROCI >4° latitude (>450 km). HK's ROCI reduced after 5 September, and its passage away from the plume region. The surface specific humidity, which is a favorable atmospheric condition for hurricane intensification (Peng and Reynolds 2006), decreased during the HK passage (<0.018 kg kg^{-1}; Fig. 7a), following an increase on the first day, while higher values were observed away from the plume region (~0.019 kg kg^{-1}). Although the humidity levels are relatively lower over the AHSW region, HK intensified, indicating that the ocean response over the AHSW region played an important role on its intensification. A strong ROCI increase is firstly observed 1 day before HM (200 km), followed by significant increase around mid-September (>400 km) (Fig. 7b). The respective humidity increased (~0.02 kg kg^{-1}), becoming a favorable condition to hurricane intensification during the HM passage over the AHSW. Humidity dropped after 9 September and especially after the passage of the TC away from the plume area. Similarly, the HO ROCI reached the 200 km level, 2 days before the storm entered the AHSW region (Fig. 7c). This indicates the potential interaction between the hurricane's winds and the upper ocean before the storm's core passed over the AHSW region. With an

exception on 26 September, the HO ROCI revealed significantly low values over the AHSW region (<100 km), supporting the argument of no intensification (relatively high MCP values, Fig. 7) and small TC size during its interaction with the plume-affected region. Although HO showed relatively high humidity levels over the AHSW region in comparison with before and after its passage (Fig. 7), its MCP revealed a strong peak (hurricane attenuation), as supported by both measured (Fig. 6c) and simulated (Fig. 7c) atmospheric fields, indicating upper ocean conditions unfavorable for intensification. Thus, the HM and HO evolution had similarities and were both different than the evolution of the preceding HK storm.

3.3 Upper ocean characteristics during August–September 2011

3.3.1 Surface temperature and salinity variability

The SST_{AHSW} evolution of August 2011 shows higher values than the respective mean 2009–2014 values (Fig. 8a). Especially in mid-August, the difference is greater than 0.5 °C, indicating that significantly warmer surface waters covered the AHSW region in 2011. The temperature levels are high when HK entered the AHSW region on 2 September (~28.5 °C). Grodsky et al. (2012), based on satellite and in situ observations, showed that the presence of the low-salinity surface layer (Amazon-Orinoco plume) inhibited mixing and warmed the ocean up to 29 °C during the passage of HK in early September 2011. The respective seasonally adjusted SST evolution is presented in Fig. 8b. HK continued to strengthen to category 4 (Fig. 6c) and to increase its size (Fig. 7a) by September 4, without revealing any strong cool wake along its track over the AHSW region. Although there is a small SST drop of 0.3 °C by 4 September (Fig. 8b), the SST levels remained high in comparison with the stronger cold wake observed a few days later (e.g., 8 September), when the SST level without the seasonal cycle was −0.2 °C. The surface temperature levels over the AHSW region were substantially high over the central and southwestern AHSW, which was covered by plume waters on 2 September 2011 (Fig. 9a). The passage of HK reduced the SST levels (~27 °C) only over the northeastern AHSW (3–4 September, Fig. 9), while the southwestern region remained significantly warmer (>28.7 °C). Large positive and high SST anomaly (ΔSST > 1 °C) between 1 day after (4 September) and 1 day before (1 September) the hurricane passage were computed over the plume area (Fig. 10a). HK caused a considerable SST cooling, which remained over the area until the HM appearance very close to the HK track. The SST difference between 8 September (HM entrance) and the mean 1–4 September period (HK passage) is generally negative (Fig. 8c), in agreement with the findings of Balaguru et al. (2014). The vast majority of the AHSW region (84 %) showed negative ΔSST (cooling) and only 16 % of the area revealed weak warming, indicating the signal of lingering wake during the first day of the HM passage over the AHSW region (Fig. 8c). Moreover, 38 % showed negative differences higher than −0.2 °C and only 2.1 % showed positive differences higher than 0.2 °C. Strong negative values (−1 °C) occurred along the HK track and especially over the northern region where HK exited from the AHSW region.

Later, the mean SST_{AHSW} gradually decreased and dropped below 28 °C on 10 September (Fig. 8a); the seasonally adjusted levels ranged around −0.3 °C (Fig. 8b). The propagation of HM across the Amazon-Orinoco plume moved the SST front westward, due to the cold wake formation below the hurricane "eye" (8–10 September; Fig. 9). The majority of the AHSW region was covered with colder waters (<28 °C) on the last day of the HM propagation on 10 September (Figs. 8a and 9c). A clear cold wake is presented in the HM ΔSST distribution over the central AHSW (<−1 °C; Fig. 10a), while low positive values are apparent only over the northeastern part of the entire AHSW region (<0.5 °C). The surface layer's temperature remained around 28 °C in the period between HM and HO, while the respective mean 2009–2014 levels are approximately 0.5 °C higher, indicating a lingering wake signal during the HO passage over the AHSW region. Similarly, the removal of the seasonal cycle reveals negative values (−0.3 to −0.4 °C) between the two hurricanes. The SST difference between 23 September and the mean values of HM passage (9–10 September) shows a strong cold wake along the HM track, indicating the presence of colder surface waters on the first day of HO (Fig. 8c). Moreover, a second significant temperature drop is simulated during the HO passage on 24 September (Fig. 8b). During the HO period, the hurricane's MCP revealed a peak over the AHSW region (~1010 hPa; Fig. 6c), while the winds were sustained at very low levels [~50 kn (NHC) and 31 kn (NOGAPS)] until the end of September (Table 1). Although the cold wake is weaker during the HO passage, surface cold waters are also evident in Fig. 9. Almost the entire AHSW region is covered with low temperature waters (<27.5 °C) on 24 and 25 September, and a clear cold wake is observed along the hurricane's track over the central and northern area (ΔSST ~ −0.8 °C; Fig. 10a). The mean ΔSST values over the AHSW region are −0.03 °C (HK), −0.362 °C (HM), and −0.13 °C (HO). The respective mean ΔSST values, derived from the daily GHRSST fields (Sect. 2.2), are −0.17 °C (HK), −0.405 °C (HM), and −0.11 °C (HO). Both model (Fig. 10a) and satellite (Fig. 10b) fields support the extensive cold wake formation during the HM passage. The relative differences between the cold wakes are also evident in maps of normalized ΔSST with respect to each hurricane's intensity (MCP) over the region (Fig. 10c). Although the HO revealed high MCP values over the region (MCP_{mean} = 1008 hPa), as derived by NOGAPS fields, and its ΔSST showed lower values in comparison with HK (MCP_{mean} = 999) and HM (MCP_{mean} = 1006), the normalized $\Delta SST/MCP_{mean}$ values for HO are close to the respective values of HM and HK, supporting the effect of weak upper ocean stratification to cold wake formation. Moreover, the cold wake

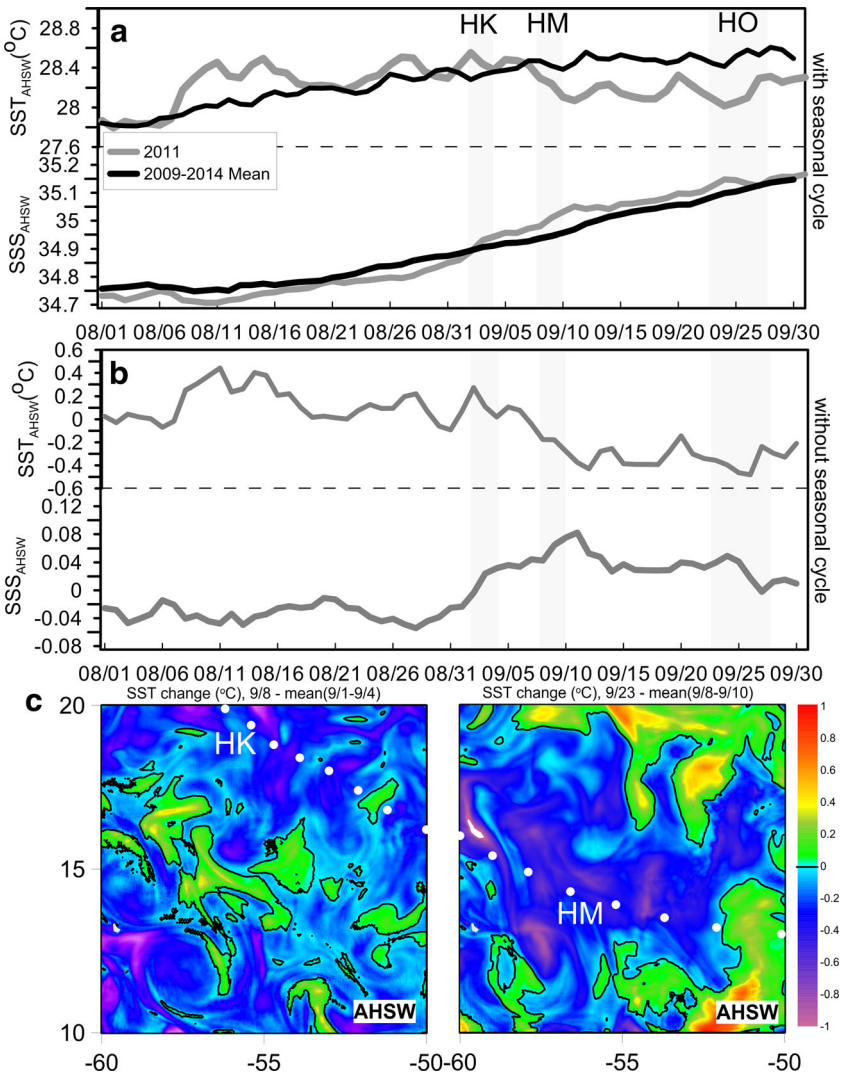

Fig. 8 Evolution of sea surface temperature (SST_{AHSW}, °C) and sea surface salinity (SSS_{AHSW}), averaged over the AHSW region (Fig. 1), **a** with and **b** without the seasonal cycle for the August–September 2011 period (*gray line*) and the respective daily mean from the 2009–2014 period (*black line*), as derived from the *Control* simulation and for Hurricanes Katia (HK), Maria (HM), and Ophelia (HO). The time period that each hurricane covered over the AHSW region is indicated with *shaded rectangles*. **c** The SST change (°C) between the first HM day and the HK mean distribution (*left panel*) and between the first HO day and the HM mean distribution (*right panel*), calculated over the AHSW region. Each hurricane's track is indicated with *white dots*

normalization with the translation speed (*ΔSST/translation speed*) revealed significantly high negative values over the central region during the HO passage, due to the low translation speed (Table 1) of the hurricane, indicating the strong HO impact over the study region (Fig. 10d). The HK translation speed is also relatively small and therefore high *ΔSST/translation speed* levels also occur over the northern region. The seasonally adjusted evolution, presented in Fig. 8b, shows that the high frequency variability noted in September 2011 is more related to hurricane effects than to seasonal variability.

We now consider the signature of the 2011 hurricanes in terms of salinity. The mean surface salinity in the AHSW (SSS_{AHSW}) is lower than usual in August 2011 (Fig. 8a). The stability of salinity levels during August is evident in the seasonally adjusted evolution of SSS_{AHSW} (~0.04; Fig. 8b). The evolution of the proportion of low-salinity waters within the AHSW area in 2011 is presented in Fig. 11c. It shows that surface waters with salinity lower than 36 cover more than 95 % of the AHSW region during August; waters with salinity less than 35.6 cover 85 % of the region. A small decrease is observed at the end of August, while a sharp drop is found during the HK intrusion on 2 and 3 of September. The coverage area of the 35.6 isohaline was reduced by 7 % within 2 days, revealing a large difference in comparison with the averaged August levels. Two respective lows of 3 and 5 % are observed for both isohalines during HM and HO periods, respectively. The coverage area trends are strong and decreasing, revealing very low p values (<0.01) according to the Mann-Kendall test of trend significance (p-values < 0.05 indicate significant trends; Mann 1945; Kendall 1975) during September (dashed lines in Fig. 11c). However, the area of low-salinity surface waters at the AHSW region showed more pronounced lows during the passages of hurricanes. In 2011, the salinity significantly increased during and after the HK passage, leading to higher values in September, compared to the 2009–2014 averaged levels (Fig. 8a). The salinity difference between early and late September is about 0.4 units (Fig. 8b). At the end of September, only 77 % of low-salinity waters (<35.6) remained over the region, almost 10 % lower than the area estimated in mid-August (Fig. 11c). Although lows are observed during each hurricane, the area reduction during HK is

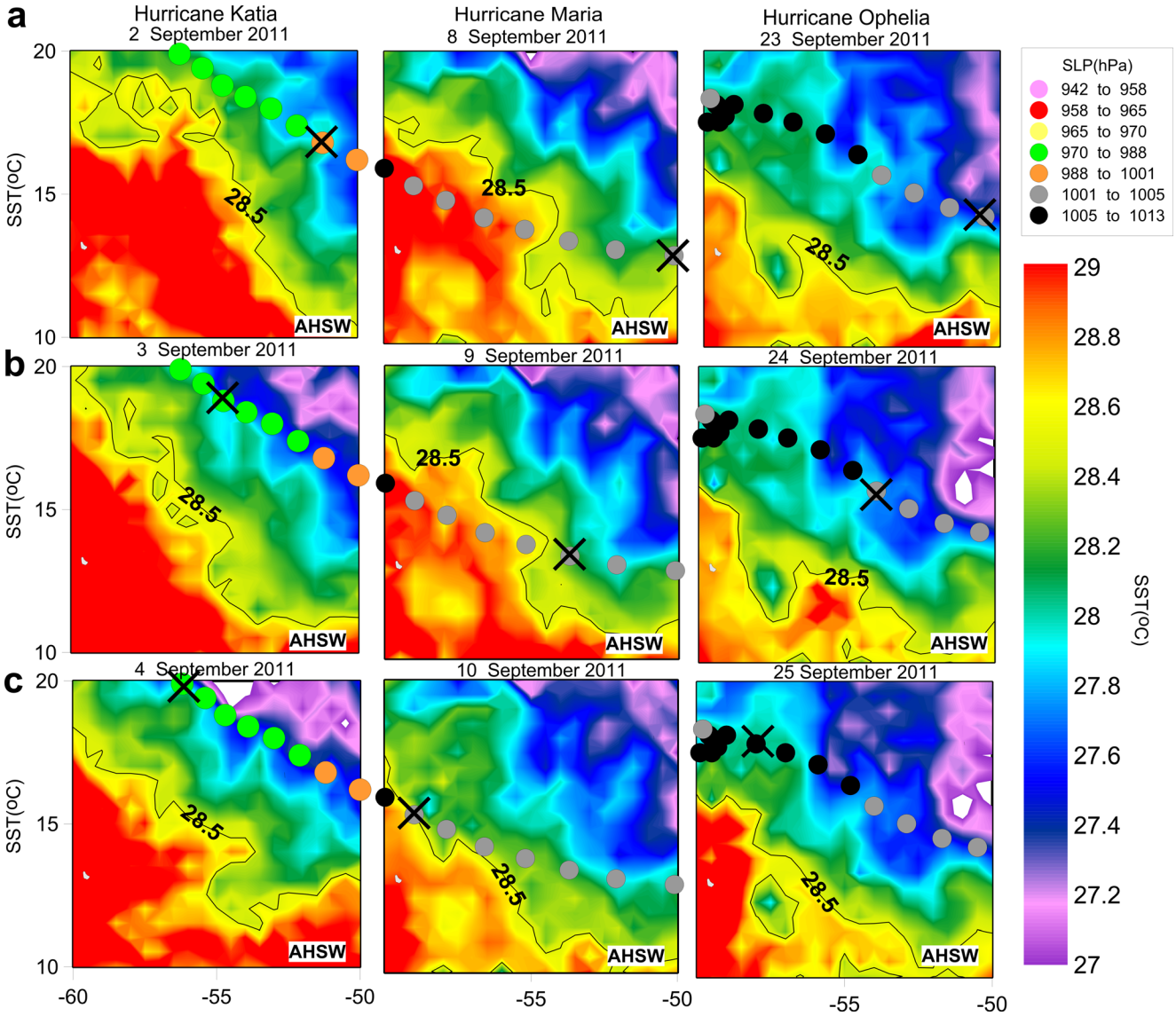

Fig. 9 Daily snapshots of sea surface temperature (SST, °C) during the hurricanes Katia (HK), Maria (HM), and Ophelia (HO) passages over the AHSW region (Fig. 1) for the following dates in September: **a** 2 (*left*), 8 (*middle*), and 23 (*right*); **b** 3 (*left*), 9 (*middle*), and 24 (*right*); **c** 4 (*left*), 10 (*middle*), and 25 (*right*) September. The respective magnitude (minimum central pressure (MCP) in hPa) and track (*circles*) of each hurricane are also shown, indicating the hurricane core's location at each snapshot date (*x symbol*). The isotherm of 28.5 °C is indicated with *solid black line*

the most intense. As expected, the precipitation rates reveal significant peaks (Fig. 11a) during each hurricane passage. In the absence of other processes, these episodes of increased precipitation in the AHSW region should reduce the surface salinity levels and increase the coverage area of low-salinity surface waters. However, salinity values increased in September 2011, especially during HM (Fig. 8a, b), suggesting the prevailing impact of the upper ocean mixing induced by the hurricane. In addition to the large precipitation associated with the three hurricanes, the trend in precipitation in September is found to be decreasing, but not statistically significant (p value = 0.29>0.05). Hence, the reduction in the area covered with low-salinity waters is due to mixing of colder and saltier waters into the mixed layer.

In addition to precipitation, we estimated the northward advection of the Amazon-Orinoco plume by computing the 100 m vertically integrated freshwater transport Q_{fw} across section S1 (10° N, 50–60° W; Fig. 1), following the freshwater transport analysis by Schiller et al. (2011) and Androulidakis and Kourafalou (2013). The freshwater transport is given by the following:

$$Q_{fw} = \int \int_{-h}^{\eta} f_{wf} \mathrm{V dz dx} \tag{4}$$

where V is the horizontal velocity normal to the section, η is the sea level, h is the 100-m depth, and the integral is

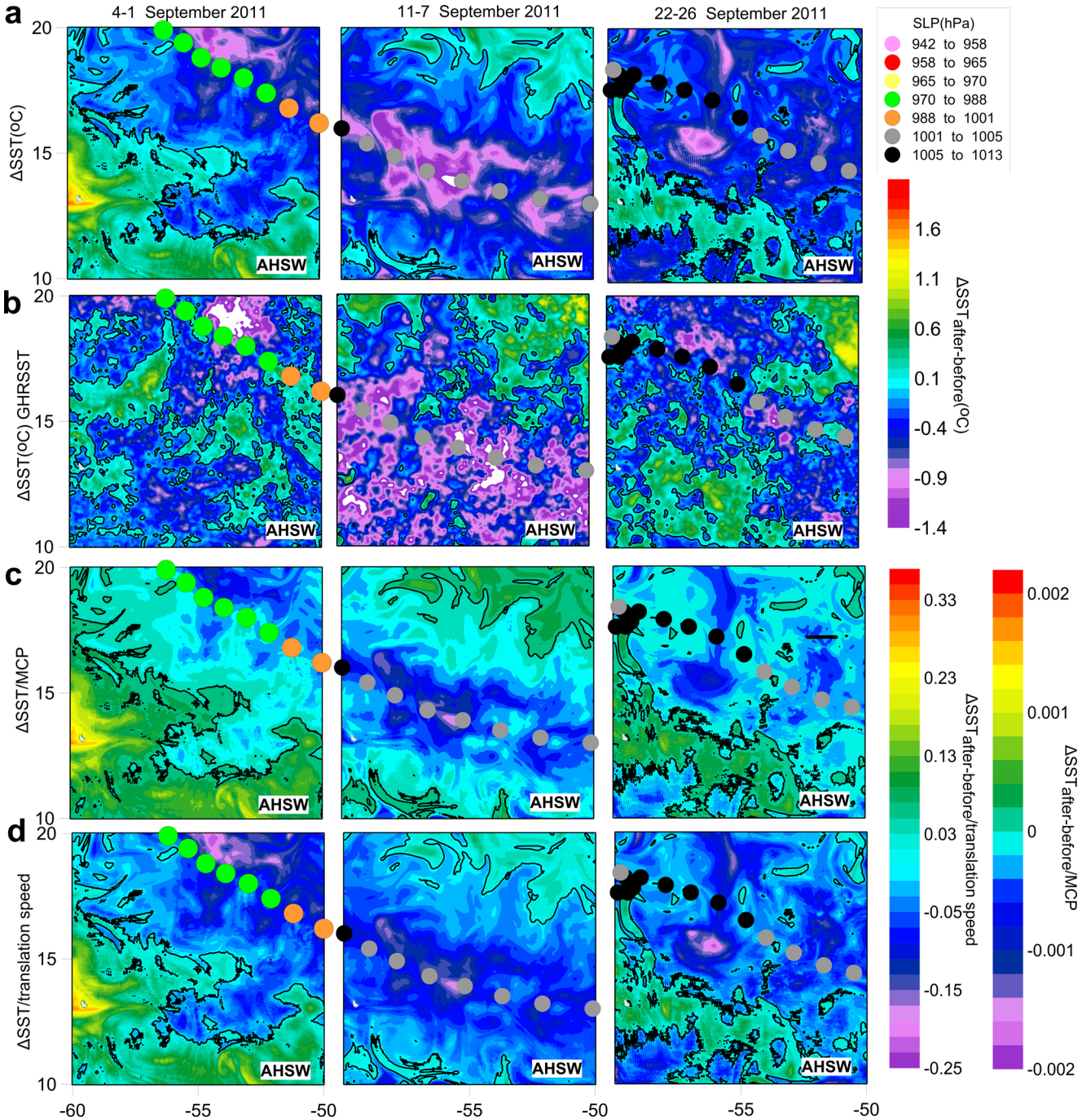

Fig. 10 Daily snapshots of sea surface temperature difference (ΔSST): **a** *Control* ΔSST, **b** GHRSST ΔSST, **c** normalized ΔSST with each hurricane's mean minimum central pressure (MCP, derived from NOGAPS), and **d** normalized ΔSST with each hurricane's mean translation speed (derived from NOGAPS) between the following dates: 4 and 1 (*left*), 11 and 7 (*middle*), and 22 and 26 (*right*) September. The respective magnitude (MCP; hPa) and track (*circles*) of each hurricane are also shown, indicating the location of the hurricane core at each snapshot date (*cross symbol*). The isotherm of ΔSST = 0, ΔSST/MCP = 0, and ΔSST/translation speed = 0 are indicated with *solid black lines*

calculated with respect to x, which is the horizontal distance along the section, as derived from the *Control* simulation. The freshwater fraction f_{wf} is calculated as $fw_f = {}^{S_b - S}/_{S_b}$, where S is the salinity from the *Control* simulation and S_b is the background undiluted salinity due to the river discharge; S_b was obtained from the twin *Noriver* simulation. V and η are estimated from the *Control* simulation. The freshwater transport gradually decreased during August, following the river discharge reduction at the end of summer, but revealed a clear increase during September (Fig. 11b). In the absence of other

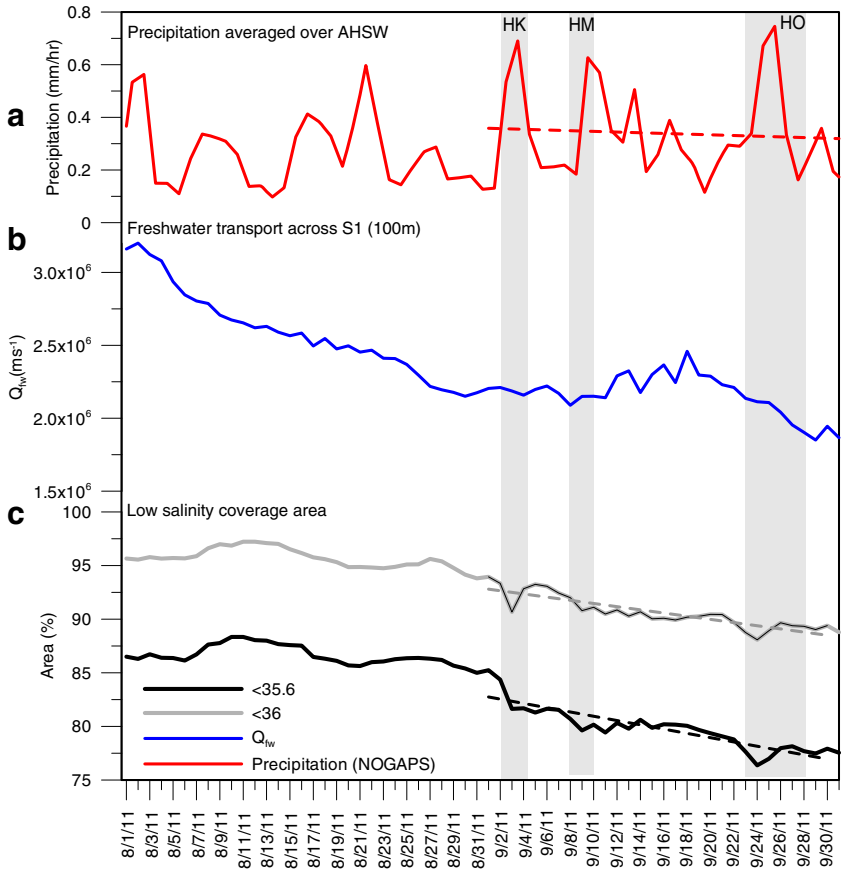

Fig. 11 Daily evolution of **a** mean precipitation (mm/h, *red line*), derived from NOGAPS fields, **b** freshwater transport Q_{fw} (m^3 s^{-1}, *blue line*) over the upper 100 m across S1 (Fig. 1), and **c** the area with sea surface salinity (SSS) lower than 36 (*gray line*) and 35.6 (*black line*) as (%) percentage of the AHSW region (Fig. 1) for August–September 2011, derived from the *Control* simulation. Positive transport values indicate northward flow. The linear trends during September are also indicated with *dashed lines*. The time period that each hurricane covered over the AHSW region is indicated with shaded rectangles (HK, Hurricane Katia; HM, Hurricane Maria; HO, Hurricane Ophelia). High (low) % denotes an effective increase (decrease) of river plume waters over the region

processes, the freshwater increase in September should be associated with an increase in the low-salinity coverage (Fig. 11c). However, this is not the case here. It thus appears that the hurricane induced mixing overcame the effects of the freshwater inputs by lateral flow and precipitation and reduced the amounts of low salinity waters over the AHSW surface.

It thus appears that the surface salinity in August 2011 was lower than usual in the area affected by the Amazon-Orinoco plume, indicating the presence of large river water quantities. At the same time, SST was anomalously warm, presumably because of this excess in low-salinity waters that impedes vertical mixing. The HK passage is associated with an increase in SSS, more pronounced than during the passages of HM and HO. Moreover, the passage of HK is associated with smaller SST, than observed for HM and HO. These differences in the temperature and salinity signature of each hurricane passage suggest an evolution of the vertical ocean structure, which is usually influenced by the presence of river waters at the surface. As shown in this section, the hurricane induced ocean mixing worked against the stratification imposed by the strong freshwater input (precipitation or ocean advection), during the sequence of events.

3.3.2 Evolution of vertical structure

Figure 12 shows the time-depth evolution of the vertical structure in temperature and salinity at various latitudes within the AHSW area. The upper layer of low salinity generally occupies the top 50 m of the AHSW region, with salinity values below 36. The central and southern part of the region reveal significantly low-salinity values (~34.5) that extend to 60 m at the 14° N–16° N latitude range to 80 m at 12° N during August 2011 (not shown). These upper waters show higher temperatures (>27 °C) than the deeper, colder layers (~24 °C). The temporal evolution of the vertical structure shows strong variability associated with the passage of hurricanes over the plume influenced region. The salinity levels of the upper ocean over the northern part of AHSW (16° N, 18° N, and 20° N) increased in the beginning of September, when HK affected that area. At 20° N, the entire upper ocean layer from 0 to 50 m was mixed with deeper water masses, leading to almost homogenous higher salinity and lower temperature values; the high pre-hurricane SST over the northern region (~28.5 °C) decreased below 27 °C during and after the HK passage. The time series of wind and surface current magnitudes are also shown in Fig. 12. The highest wind speed of the entire study period (>20 m s^{-1}) was observed during the HK

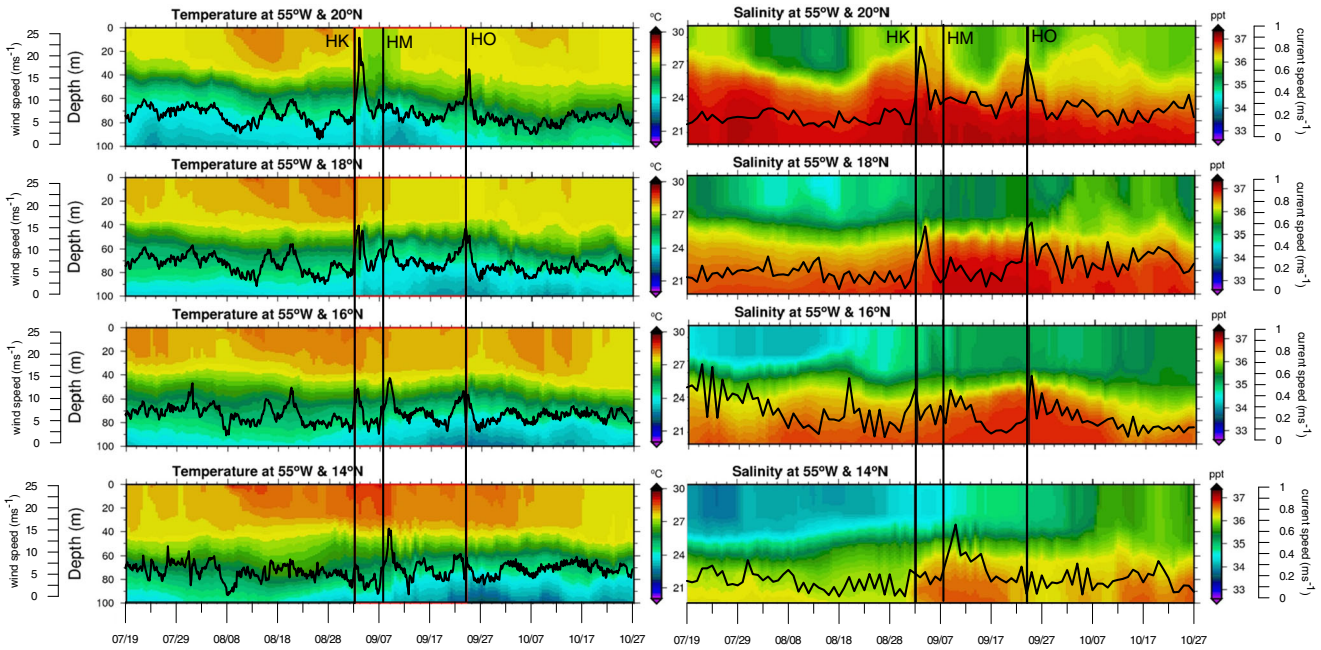

Fig. 12 Temporal evolution of vertical distribution of temperature (*left*) and salinity (*right*) over the upper 100 m at latitudes 14° N, 16° N, 18° N, 20° N along the 55° W meridian in the *Control* simulation. The wind (*left panels*) and surface current speed (*right panels*) evolutions derived from NOGAPS and *Control* run at each latitude are also presented (*black solid lines*). The dates when Hurricane Katia (HK), Hurricane Maria (HM), and Hurricane Ophelia (HO) entered the AHSW region (Fig. 1) are indicated with *black solid lines*

intrusion at 20° N latitude. A strong surface current speed peak (>0.8 m s^{-1}) was also observed at the same location. Comparable changes took place at 16° N and 18° N, where salinity increased and temperature decreased during the HK passage. Strong outer winds and currents were observed along the entire 55° W (wind speed and current increase during HK intrusion at all sections) indicating the hurricane's impact over the entire AHSW region. At 20° N, the ocean started to restratify soon after HK, as seen in both the temperature and salinity sections. At 18° N and 20° N, the HK passage enhanced the cooling of the surface layer by bringing colder and saltier water from below 50 m to the mixing level. Then, between 14° N and 18° N, the passage of HM and its accompanying strong winds (>10 m s^{-1}) led to an increase of current magnitude and to a cooling in mixed layer temperature, without noticeable changes in mixed layer salinity. Finally, the passage of HO was associated with the cooling of the upper layer at 16° N, but its signature at other latitudes or in temperature was not marked. The passage of HK was thus associated with mixing and upwelling that modified the ocean vertical structure before the passages of HM and HO.

Near-inertial waves also contribute to the upper ocean mixing in the days following the passage of a hurricane (Price 1981). Signals of near-inertial waves are observed in temperature, at the base of the mixed layer, especially after the HM passage (Fig. 12). To investigate the near-inertial response, the evolution of the current components was computed at mixed layer depth (MLD; the MLD computation is described in Sect. 4.2) at several locations along 55° W (Fig. 13). Although no significant inertial wave is observed in August before the hurricane activity (Figs. 12 and 13), with the exception of 16° N, the detided time series (the *Control* simulation does not include tides) revealed energetic oscillations after each hurricane passage. This is in agreement with observations by Shay et al. (1998), who found similar response due to the Hurricane Gilbert passage in the western Gulf of Mexico. The northern part of the region (18° N and 20° N), located below and to the right of the HK track, shows strong oscillations with amplitude of 80 cms^{-1}, while the oscillations were sustained but with weaker signal after HM (~20 cms^{-1}). After the HM passage, the currents at the center of AHSW (14° N) were increased (20 cms^{-1}) between 10 and 18 September. Finally, near-inertial oscillations with amplitudes around 60 cms^{-1} are observed during and after the HO passage over 18° N for both components of the current at the bottom of the mixed layer (Fig. 13), confirming the presence of near-inertial waves, as indicated from the temperature vertical section at 40-m depth (Fig. 12).

4 Discussion

The upper ocean stratification over the AHSW region is strongly related to the northward spreading of the Amazon-Orinoco plume and plays an important role in the air-sea interaction processes during the TC propagation. We computed

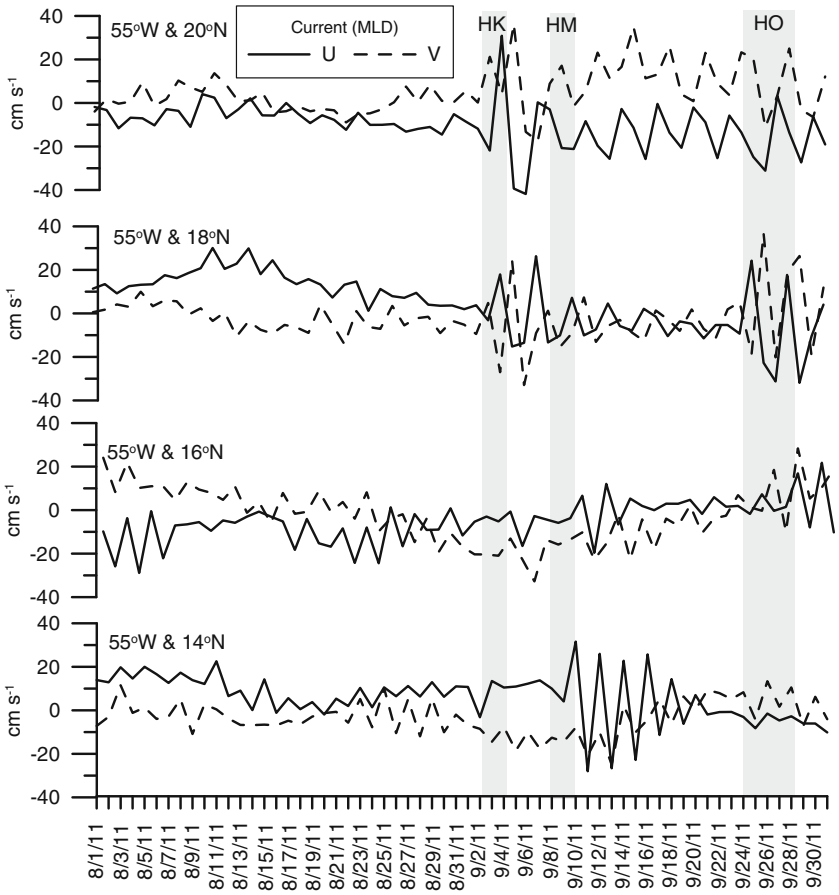

Fig. 13 Evolution of U (*solid*) and V (*dashed*) current component (cms^{-1}) at mixed layer depth (MLD) of 14° N, 16° N, 18° N, 20° N latitudes along the 55° W meridian in the *Control* simulation. The time period that each hurricane covered over the AHSW region (Fig. 1) is indicated with *shaded rectangles* (HK, Hurricane Katia; HM, Hurricane Maria; HO, Hurricane Ophelia)

the evolution of the stratification frequency of the upper ocean, the BLT variability, the thermal potential, and the cooling resistance of the plume region in order to discuss the hurricane-ocean interaction over this plume affected area of the western Atlantic Hurricane region during August and September of 2011.

4.1 Upper ocean stratification

The stratification frequency (Brunt-Väisälä frequency; Eq. 5) of the upper ocean is computed in order to investigate the vertical mixing ability of the water masses located between 0 and 100 m.

$$N = \frac{\left(-g \Big/ \rho_o\right)(\rho_1 - \rho_2)}{\Delta z} \tag{5}$$

where g is the gravitational acceleration (9.806 m s^{-2}), ρ_o is the initial ambient sigma-theta (1022.4 kgm^{-3}), ρ_1 and ρ_2 are the upper and lower layer mean density, respectively, and Δz is the thickness of each model layer in order to calculate the mean stratification frequency of the upper 100 m. The daily stratification frequency N is averaged over the AHSW region during August–September 2011 (black solid line in Fig. 14). The stratification frequency N is estimated for both *Control* ($N_{Control}$) and *Noriver* ($N_{Noriver}$) simulations.

Peaks of $N_{Control}$ stratification are found around 10 August, mid-August and late-August, while the highest September values are observed on the first day of the HK passage (2 September). This indicates the strong stratification of the plume area due to the presence of the low-salinity layer, in agreement with the temperature and salinity vertical distribution presented in Fig. 12. The differences between the surface salinity and salinity at 100 m ($dS = SSS\text{-}S_{100}$) are also shown in Fig. 14. Very large differences in the *Control* simulation ($dS_{Control} > -0.8$) also indicate the presence of a strong buoyant plume at the surface of the region during August. In particular, $dS_{Control}$ levels around −0.84 are found during a short period before the HK intrusion (27 August–1 September). In the *Noriver* simulation, the respective $N_{Noriver}$ values are significantly lower, indicating the weaker stratification and smaller dS differences (highest value of $dS_{Noriver}$ is −0.55) occurred in the absence of river plume. HK mixed the upper low-salinity layers and reduced both the stratification frequency and $dS_{Control}$ during the 2 days of the storm interaction with the brackish plume, in agreement with Grodsky et al. (2012), who used satellite salinity measurements and showed that HK increased the SSS over the plume area. For the year 2011, the Pearson correlation coefficient between the $N_{Control}$ frequency

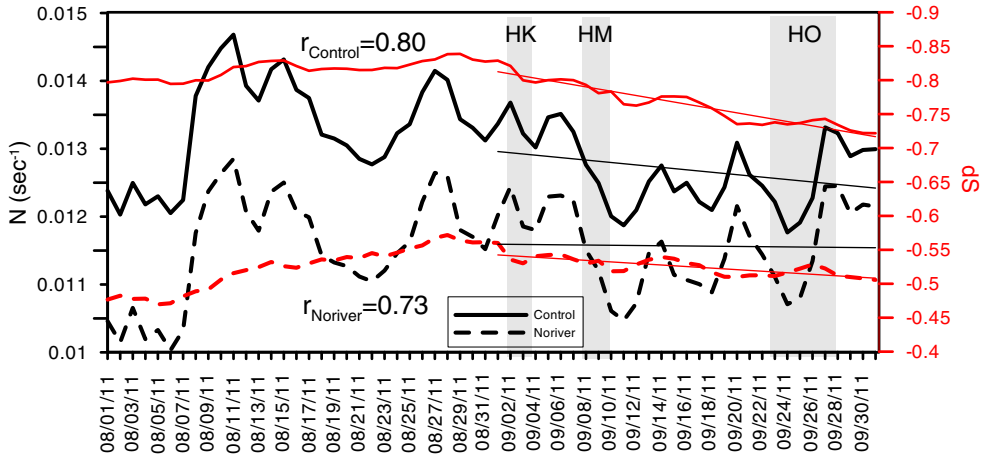

Fig. 14 Evolution of daily difference between sea surface salinity (SSS) and salinity at 100 m (dS = SSS-S_{100}; *red line*) and stratification frequency N (s^{-1}) over the upper 100 m (*black line*), averaged over the AHSW region (Fig. 1). All temporal evolutions refer to the August–September 2011 period, as derived from both *Control* (*solid line*) and *Noriver* (*dashed line*) simulations. The Pearson correlation coefficient (r) between N and dS for each experiment, computed for 2011, and the linear fit (*thin lines*) for each time series during September 2011 are also presented. N represents all simulated values along the 100-m water column. The time period that each hurricane covered over the AHSW region is indicated with *shaded rectangles* (HK, Hurricane Katia; HM, Hurricane Maria; HO, Hurricane Ophelia)

and the $dS_{Control}$ salinity difference is high and close to 1 ($r_{Control}$ = 0.80; Fig. 14), indicating the good correlation and strong interaction between upper ocean stratification and surface salinity variability over this hurricane and river plume affected region. The respective coefficient in the *Noriver* case is lower due to the absence of the plume, which plays an important role on the upper ocean stratification ($r_{Noriver}$ = 0.73). The decrease in $N_{Control}$ in September is also related to both salinity increase and temperature reduction over the upper 50 m, as seen in Fig. 12. Although the stratification of the upper 100 m weakened significantly after the HK passage over the plume on 4 September, $dS_{Control}$ remained constant in the short period between HK and HM (~0.80), supporting a temporary peak of $N_{Control}$. However, the intrusion of HM further reduced the $dS_{Control}$ levels and the $N_{Control}$ frequency, which finally reached its lowest levels (<0.012 s^{-1}) right after the passage of the storm's core over the region. As presented in Sect. 3.3.1, mean SST values decreased and mean SSS values increased, indicating the intense mixing of the upper ocean before and during the HM passage over the plume area. The less stratified upper ocean allowed the SST cooling and thus helped to inhibit the intensification of HM (Fig. 6c), in agreement with Sengupta et al. (2008), Wang et al. (2011), and Balaguru et al. (2012a). Very low $dS_{Control}$ values (less of ~0.74) and the lowest $N_{Control}$ levels (~0.0117 s^{-1}) of the entire period were found during the HO passage on 24 September, indicating a weak resistance to mixing and thus favoring the cooling of the upper layers, supporting the low intensity (~1000 hPa, Fig. 6c) and the small ROCI (<200 km, Fig. 7c) of the hurricane during its passage over the plume region. The combination of the upper ocean structure during HO and its low translation speed (<3 m s^{-1}, Fig. 6c) supported the increase of HO MCP on 25 September 2011.

In September 2011, $dS_{Control}$ revealed a larger range of values (>0.10 difference between 1 to 30 September) than $dS_{Noriver}$ (~0.05; weaker reduction), associated with the mixing of plume waters with deeper waters and the associated increase in surface salinity induced by the hurricanes. As a result, the linear fit of dS for the *Noriver* experiment has a much smaller slope than in the *Control* experiment. Similarly, the stratification frequency in the *Noriver* experiment revealed similar values before and after the hurricanes impact and does not show any decreasing trend during September 2011, as in the *Control* experiment. The analysis of the stratification frequency and the salinity stratification in the *Control* and *Noriver* simulations, thus illustrate the impact of the river plume in the upper ocean structure of the AHSW region and its evolution under the influence of hurricanes.

4.2 Barrier layer thickness detection and evolution

According to Masson and Delecluse (2001), the halocline formed by the Amazon-Orinoco waters is located at 40-m depth and is present every summer north of the Amazon mouth. Moreover, Pailler et al. (1999) argued that the river discharge may induce a strong halocline and thus an apparent low-salinity layer over the surface in the 3–30-m depth range. This halocline induces a pycnocline that acts as a barrier for mixing between the surface and the subsurface waters. The estimation of the BLT over the Amazon affected region is related to the MLD estimation, based on a variable sigma-t (σ_t) criterion, and to the computation of the isothermal layer depth (ILD) (Sprintall and Tomczak 1992). The sigma-t criterion determines the depth where σ_t is equal to the surface σ_t plus the

increment in density equivalent to a specific decrease in temperature (ΔT).

$$\Delta\sigma = \sigma_t(SST-\Delta T, SSS)-\sigma_t(SST, SSS) \quad (6)$$

where $\Delta\sigma$ is the difference in density from the surface to the base of the MLD. ΔT is set equal to 0.3 °C, and salinity is constant and equal to SSS. The MLD is found by detecting the depth, where σ_t is equal to surface σ_t plus $\Delta\sigma$ (Felton et al. 2014; MLD criterion). The BLT is the difference between the ILD and MLD (BLT = ILD − MLD). The ILD is found by detecting the depth, where temperature is equal to SST-ΔT (ILD criterion). Any difference between those two criteria will then only be due to salinity stratification, and this will provide an estimate of the BLT (De Boyer Montégut et al. 2004, 2007).

The horizontal distribution of MLD on the first day of each hurricane over the AHSW region is presented in Fig. 15a. Stabilizing brackish waters of the plume led to the computation of small MLD during the intrusion of HK over the AHSW region and especially over the southwestern plume area, where the mixed layer is smaller than 10 m. In addition, Fig. 15b presents the evolution of BLT, ILD, and MLD in the meridional center (55° W) of the northern AHSW region, averaged in the range 18° N–20° N for HK, 14° N–16° N for HM and 16° N–18° N for HO, in order to focus over each area that was mainly affected by the three successive hurricanes in September 2011. BLT and MLD ranged between 20 to 30 m in late August, before HK entered the region (Fig. 15b). The hurricane passage over the northern AHSW area decreased the BL thickness by 17 m (11 m on 3 September; Fig. 15b). This low is associated with the respective thermocline deepening, the increase of the ILD to 52 m after the HK passage (5 September), and the increase of the MLD by almost 20 m. The lowest BLT occurred on 3 September, when a MLD peak occurred (from 20 to 40 m), indicating the importance of the salinity stratification. Although a reduction in MLD is observed at 14° N–16° N, 1 day before the HM appearance (7 September; Fig. 15b), it is located in a small area over the central AHSW region (Fig. 15a), away from the location of HM entrance. The BLT was still large on 6 September (~28 m; Fig. 15b), but it started decreasing gradually during the HM approach toward the region and finally dropped to almost 10 m when the HM "eye" crossed over the central AHSW area (14° N–16° N). The BL shrinkage favored the mixing of the upper ocean with colder upwelling waters and thus the increasing of both ILD and MLD, in comparison with the shallow levels of August. Larger MLD (>30 m) is present over almost the entire AHSW region on 8 September, indicating the extensive vertical mixing that took place during and after the HM passage (Fig. 15a). The ILD follows the MLD distribution during HM, while the BLT is small due to its erosion during the previous and current hurricanes. The BLT was low over the central AHSW region (<20 m Fig. 15b) after HM (11 September), and remained low and constant during HO (~15 m; Fig. 15b). The BLT ranged around 10 m on 25 September, when the storm's core was over the northern plume region (Fig. 9c). The respective MLD ranged between 35 and 40 m, indicating the large mixing layer that formed during HO in comparison with the lower levels observed before the HK and HM hurricanes (~20 m). Although no strong alterations of the MLD and ILD are observed during HO over 16°–18° N (Fig. 15b), a thick mixed layer (~40 m) covered the entire region on 23 September, when HO appeared (Fig. 15a). There is a clear difference between the BLT variations before and after the HK passage. The lower BLT values (~10 m), which prevailed after HK, allowed the cooling of the surface layers due to HM and HO influence. There is a deepening of the MLD, especially during HK and HM, while it remained deeper than 35 m almost for the entire month, indicating strong mixing processes.

4.3 Thermal potential of the upper ocean

The potential effect of upper ocean stratification on hurricane intensity is estimated by comparing several oceanic metrics used to study TC intensity. SST variability, which is presented in Sect. 3.3.1, is a basic predictor for the potential intensity of a hurricane (Emanuel 1987). Moreover, in order to describe the interaction of the hurricane with the ocean subsurface, we computed the averaged temperature of the upper 100 m (T_{mean100}; Price 2009) and the difference between the SST and temperature at 100 m (dT_{100} = SST − T_{100}), which is a typical depth of vertical mixing by hurricanes. The integrated ocean heat content above the 26 °C isotherm (Leipper and Volgenau 1972) is also called *TCHP* (Jcm^{-2}):

$$\mathrm{TCHP} = C_p \int_{z_{26}}^{0} \rho(z)(T(z)-26)dz \quad (7)$$

where z_{26} is the depth (m) of the 26 °C isotherm, $C_p = 4.0 \times 10^3$ J kg^{-1} °C^{-1} is the heat capacity, $\rho(z)$ and $T(z)$ are derived from the simulated sea density (kg m^{-3}) and temperature (°C) distributions between z_{26} and surface. *TCHP* is used extensively by the National Oceanic and Atmospheric Administration (NOAA) for hurricane forecasts (Newinger and Toumi 2015). In addition, the depth of the 26 °C isotherm (H_{26}) is also considered an important predictor of the TC evolution and intensity (Goni et al. 2003). All thermal metrics are averaged over the AHSW hurricane-plume region in order to examine the specific contribution of the BL during the hurricane passages.

The highest peak of mean temperature during all summer, averaged over the upper 100 m, is observed on 2 September in the *Control* simulation (T_{mean100} = 26.73 °C; Fig. 16a). A

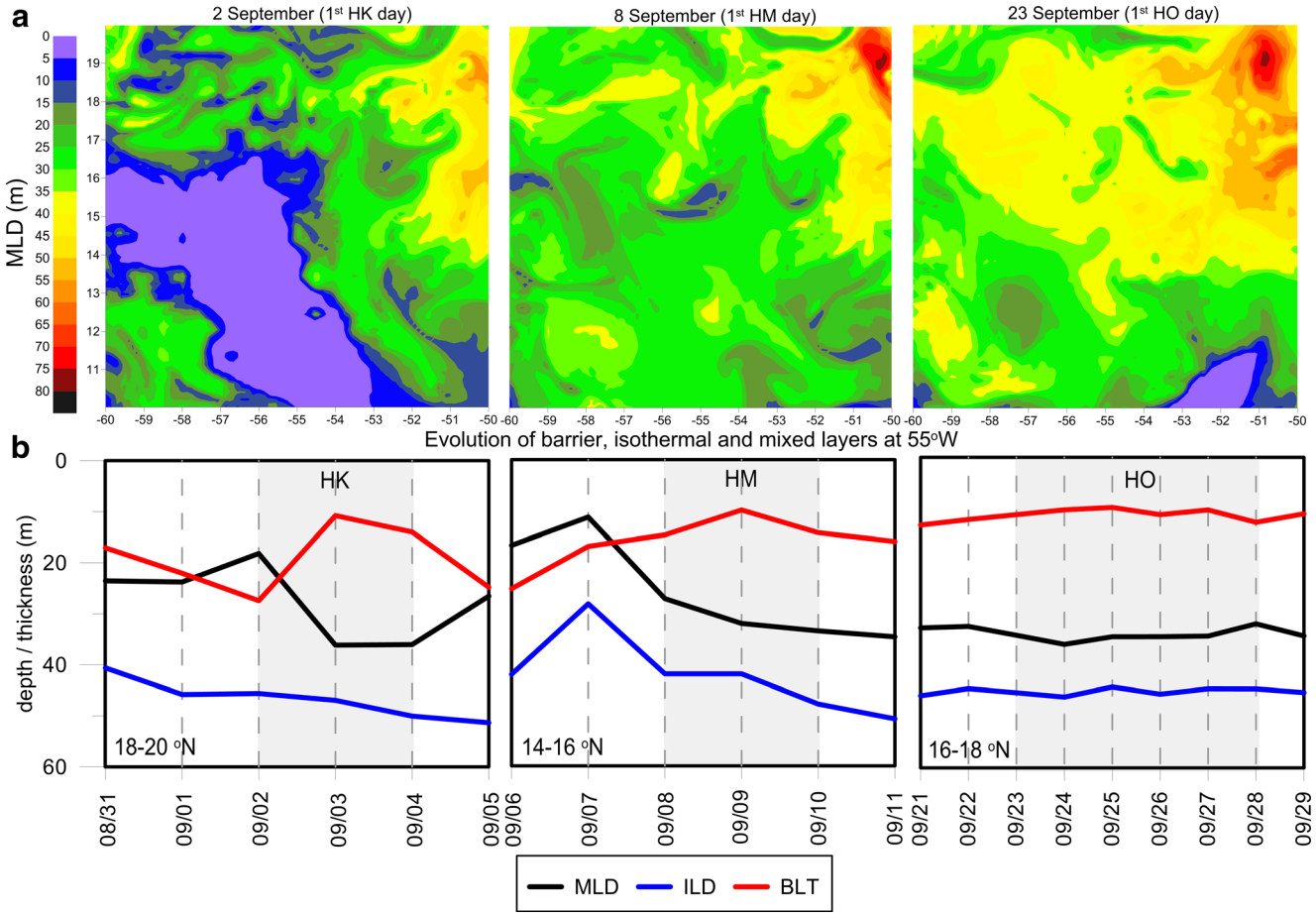

Fig. 15 **a** Horizontal distribution of mixed layer depth (MLD) on the first day of each hurricane over the AHSW region (Fig. 1): *left*, 2 September; *middle*, 8 September; *right*, 23 September. **b** Evolution of daily MLD, isothermal layer depth (ILD) and barrier layer thickness (BLT) averaged at 55° W between 18° and 20° N (HK), 14° and 16° N (HM), and 16° and 18° N (HO), as derived from the *Control* simulation. The time period that each hurricane covered over the AHSW region is indicated with *shaded rectangles* (HK, Hurricane Katia; HM, Hurricane Maria; HO, Hurricane Ophelia)

strong reduction took place during the HK period (2–4 September), which also continued during the HM period (until 10 September). Similarly, the dT_{100} difference is almost 0.5 °C lower a day after the HM passage (11 September), indicating the cooling of the surface layers during the previous 10 days. A continuous reduction of both upper mean temperature and the difference between surface and 100-m depth took place until the HO intrusion over the area, confirming the formation of a lingering cold wake between the first (HK), the second (HM), and the third (HO) hurricane (Fig. 8c). Both time series reveal a significant low on 26 September, while the HO core was over the plume-affected region. The high T_{mean100} values in the beginning of the HK passage over the region supported the intensification of the storm (Fig. 6c) and its size increase (Fig. 7a). However, the decrease of the temperature metrics after HK and especially during the HM and HO periods is an indicator of reduced thermal energy that hurricanes were able to draw from the upper ocean layers.

The characteristics of the low-salinity layer determine the evolution and levels of all metrics before, during, and after a hurricane passage. The *Noriver* experiment (Sect. 3.1), where river plume is totally absent, revealed shallower H_{26} and lower *TCHP* levels over the AHSW region during August and September 2011 (Fig. 16b). Large (deep) H_{26} values indicate a larger volume of warm waters that may supply energy to potential storms. The absence of BL in the *Noriver* case is associated with a large difference between the two H_{26} time series (4 to 10 m difference). The presence of a BL in the *Control* case kept the upper ocean warmer and favorable to hurricane intensification. The heat addition (solar warming) to the upper ocean during August deepened the H_{26} isotherms for both *Noriver* (from 28 to 34 m, Fig. 16b) and *Control* (from 32 to 42 m, Fig. 16b). The presence of a BL led to a larger deepening of the 26 °C isotherm in the *Control* experiment. However, the weakening of the BL during HK and HM due to hurricane induced

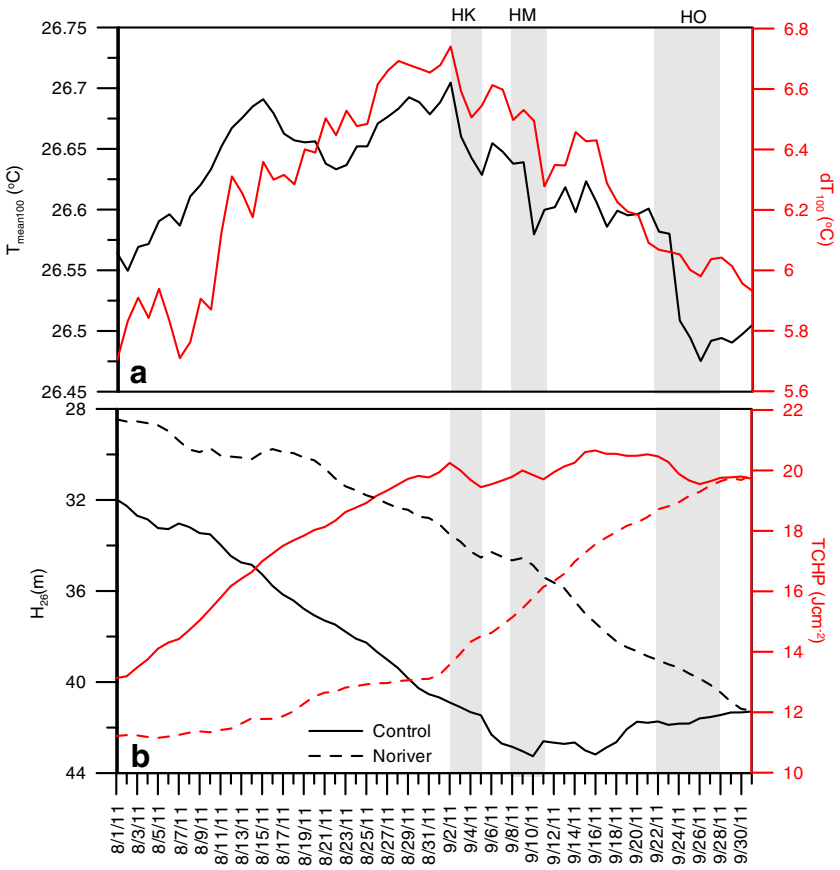

Fig. 16 Evolution of **a** daily averaged temperature of the upper 100 m ($T_{mean100}$, *black line*) and differences between sea surface temperature (SST) and temperature at 100 m (dT_{100}; *red line*), and **b** depth of the 26 °C isotherm (H_{26}, *black line*) and tropical cyclone heat potential (*TCHP*, *red line*), averaged over the AHSW region (Fig. 1). All temporal evolutions refer to the August–September 2011 period, as derived from the *Control* (*solid line*) and *Noriver* (*dashed line*) simulations. The time period that each hurricane covered over the AHSW region is indicated with *shaded rectangles* (HK, Hurricane Katia; HM, Hurricane Maria; HO, Hurricane Ophelia)

mixing inhibited the farther deepening of the H_{26} isotherm, which stayed constant and even reduced its depth (~2 m) during September. Similarly, the hurricane impact is apparent in the H_{26} evolution of the *Noriver* simulation, especially in the HM case; the hurricane passage temporarily interrupted the H_{26} deepening at 34.5 m (small peak on 10 September).

The *TCHP* values in the *Control* simulation, averaged over the AHSW region, increased in August and reached a peak of 20 J cm^{-2} on 2 September 2011, during the intrusion of HK's eye in the region. A direct small decrease took place in the following two days (2–4 September), while the *TCHP* levels remained almost constant during the entire September (~20 J cm^{-2}), without showing any additional increase in comparison with the *Noriver TCHP*, which increased continuously. The *TCHP* levels are always lower in the *Noriver* case, because the absence of the plume (and associated BL) implies a less stratified upper ocean, which favors stronger upper ocean mixing and reduced heat content for hurricane intensification. The less stratified upper ocean (lower $N_{Noriver}$ frequency; Fig. 14) is associated with a weaker response to the hurricane passages. Therefore, the *TCHP* levels in the absence of river plume are not strongly affected by the passage of a hurricane, although the slope of the increasing trend in *TCHP* became steeper after HK. Both H_{26} and *TCHP* metrics ranged over the same levels (~20 m and ~12 J cm^{-2}) for both simulations (*Control* and *Noriver*) at the end of September, after the passages of the three hurricanes.

The anomalous surface warming effect of vertical mixing is already present in the heat content-based metrics in the case of strong salinity stratification (Price 2009), like the Amazon-Orinoco plume. However, the use of metrics that take into account the density stratification provides better description of the ocean-hurricane interaction and the vertical mixing of the upper ocean (Newinger and Toumi 2015). Therefore, we used the cooling inhibition (*CI*) index, introduced by Vincent et al. (2012) in order to measure the potential energy (ΔE) required to cool the ocean surface (e.g., by 2 °C) through mixing by taking into account both thermal and haline stratification (Eq. 8).

$$\Delta E(-2^{o}\mathrm{C}) = \int_{h_m}^{0} (\rho_{2C} - \rho_i(z))\mathrm{gzdz} \tag{8}$$

where ρ_i is the initial profile of density, simulated by the model, z is the ocean depth coordinate, ρ_{2C} is the homogenous final density profile after mixing, with constant temperature inside the mixed layer equal to SST_i-2 °C. The mixing depth h_m that is necessary to produce a 2 °C cooling, is computed

from the equation of conservation of heat. Vincent et al. (2012) defined *CI* as the cube root of the necessary potential energy to induce a 2 °C SST cooling:

$$CI = [\Delta E(-2^{o}\mathrm{C})]^{1/3} \quad (9)$$

High *CI* values indicate resistance of the ocean to surface cooling though mixing. The wind and surface current distribution on characteristic dates before, during, and after the HK passage are presented in Fig. 17.

Prior to the storm (Fig. 17a), strongest currents are evident within two anticyclones in the southwestern part of the domain (Fig. 17b). The anticyclones are prominent features of the oceanic circulation and have propagated from the South, along the Brazil Current (Fig. 17c). These eddies are known as Brazil Current rings (Fratantoni et al. 1995; Goni and Johns 2001); the signature of the northeastward flowing Northern Brazil Current (NBC; Fig. 17c) is actually evident along the southern ring within AHSW (Fig. 17b) and is the cause of the deeper MLD in Fig. 15. When the hurricane eye has fully entered and the hurricane winds have influenced most of the AHSW (2 September), strong currents have developed in the northeastern to southeastern study area, in an overall cyclonic pattern. As the storm exits (5 September), strong currents are still evident in the northern AHSW, as remnants of the hurricane influence. The horizontal distribution of SSS and *CI* for both *Control* and *Noriver* cases on the same dates as in Fig. 17 are presented in Fig. 18. The lowest SSS values (Fig. 18a) are observed within the two southern anticyclones, which apparently are carrying

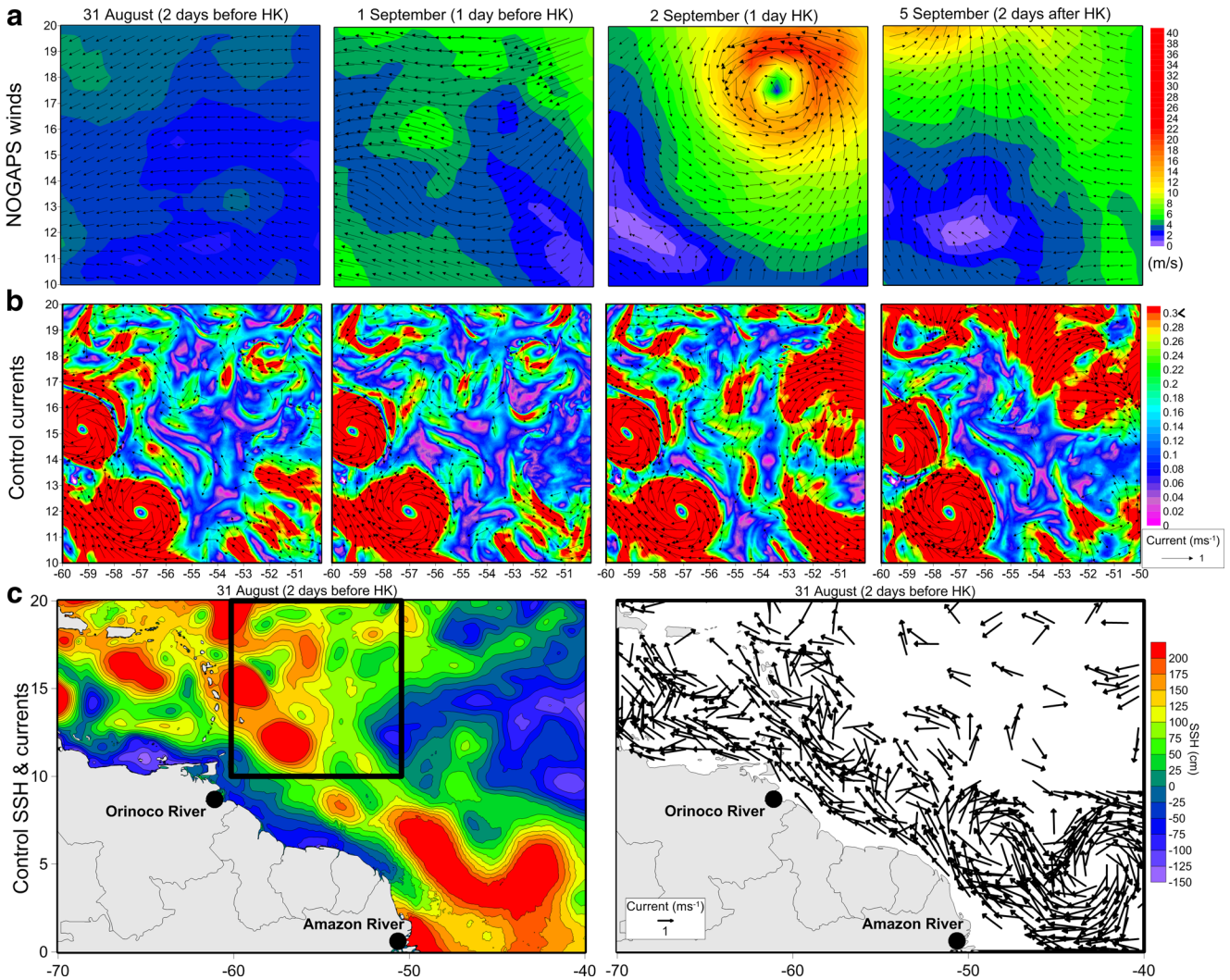

Fig. 17 Horizontal distribution of **a** wind speed and vectors and **b** surface current velocity and vectors (*red colors* show current magnitudes speeds exceeding 0.30 m s^{-1} and vectors below 0.15 m s^{-1} are excluded) over the AHSW region (Fig. 1) on 31 August 2011 (*left*), 1 September 2001 (*middle-left*), 2 September 2011 (*middle-right*), and 5 September 2011 (*right*). **c** Horizontal distribution of sea surface height (SSH, cm) and surface current vectors over an extended region on 31 August 2011. The Orinoco and Amazon locations and the Atlantic Hurricane SouthWestern (AHSW) subregion are indicated with *big black dots* and a *black square*, respectively

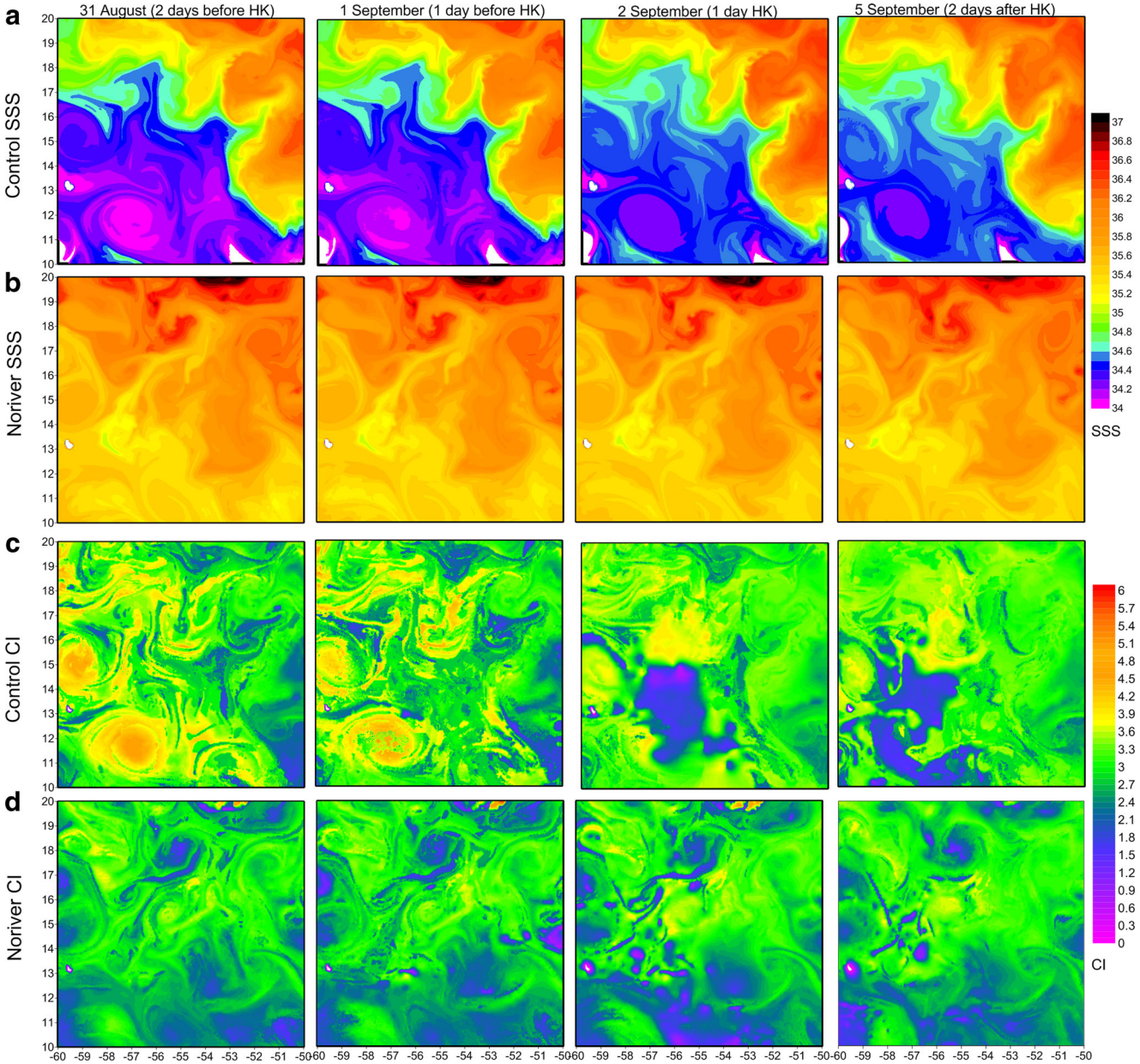

Fig. 18 Horizontal distribution of **a** *Control* sea surface salinity (SSS), **b** *Noriver* SSS, **c** *Control* cooling inhibition (*CI*) index, and **d** *Noriver CI* index over the AHSW region (Fig. 1) on 31 August 2011 (*left*), 1 September 2011 (*middle-left*), 2 September 2011 (*middle-right*), and 5 September 2011 (*right*)

Amazon waters in the surface layers toward the Caribbean Sea (Muller-Karger et al. 1988, 1995; Ffield 2005, 2007). However, Ffield (2007) showed that strong winds from hurricanes might quickly obliterate a thin plume, exposing several-degrees-cooler NBC ring water to the surface, and potentially contributing to rapid cooling of the surface and thus to hurricane attenuation. Low SSS values over a broader area indicate the full extent of the plume region. As expected, SSS in the *Noriver* case (Fig. 18b) has a more homogeneous distribution with overall higher SSS. High *CI* values are reached in the *Control* simulation on 31 August (Fig. 18c), 2 days before the HK eye entered AHSW and the storm reached the plume region (Fig. 17a). The entire river plume region in the central and southwestern area reveals *CI* values over 3, indicating a strong resistance of the upper ocean to cooling 2 days before the eye of the cyclone passes over the study region. Similarly, the upper ocean resistance remains strong one day before the HK entrance (1 September 2011). The highest *CI* values are observed in the lowest SSS areas, mainly inside the two anticyclonic eddies.

Based on the above findings from our *Control* simulation, the river-induced stability due to increased stratification clearly enhanced the HK intensity, associated with high *CI* levels. Our results are in agreement with Balaguru et al. (2012a), who

showed that the BL may reduce storm-induced vertical mixing and SST cooling, causing an increase in enthalpy flux from the ocean to the atmosphere and, consequently an intensification of tropical cyclones. On the contrary, lower values are observed in the *Noriver* simulation on both days before the hurricane passage (*CI* < 2.7, Fig. 18d). The absence of river plume waters (high SSS; Fig. 18b) and BL causes weak resistance of the upper ocean to mixing due to hurricanes (low *CI* levels). Newinger and Toumi (2015) showed that the river plume brackish waters prevent the sunlight from reaching deep in the ocean, leading to moderate surface warming and substantial subsurface cooling. Consequently, they claim that relatively cold water below the mixed layer is more readily available to passing storms, which would reduce their intensity and be associated with low *CI* levels. Although water turbidity was not included in our purely hydrodynamic modeling, we deduce that this might be a secondary effect in our study, as the hurricane influence took place in the outer part of the river plume area, where turbidity is relatively reduced. Having established the relationship between *CI* and the river plume region, we examine changes due to the hurricane passage. First, we focus on the relationship of *CI* with oceanic properties. The intrusion of the HK over the region on 2 September and the erosion of the BL (increase in SSS, Fig. 18a) led to the weakening of the ocean's resistance to mixing and revealed an area of low *CI* values (<0.5), especially over the central AHSW and northeastern part of the plume region (Fig. 18c). The high *CI* values within the anticyclonic rings also eroded gradually, following an increase in SSS. The overall SSS increase (that caused the *CI* reduction) is in agreement with the restriction of the area covered by SSS values of 35.6 computed during the HK intrusion on 2 and 3 of September (Fig. 11c). We have shown that strong outer winds were observed along the entire 55° W meridian due to the passage of HK over AHSW (Fig. 12). More specifically, strong cyclonic winds occurred on 2 September (Fig. 17a), when the HK core propagated over the northeastern AHSW and the storm covered the majority of the study area, including the eastern part of the plume affected region (central AHSW). These winds exceeded 20 m s^{-1} close to the hurricane's core and remained relatively high over the 14° N latitude (~8 m s^{-1}; Fig. 17a) in agreement with the 41040 buoy observations presented in Fig. 2a. The evolution of wind speed at 14° N showed three distinctive peaks during HK, HM, and HO passages over the AHSW region (Fig. 12). Strong surface currents appeared over the northeastern region, below the HK track (Fig. 17b). It seems that the HK passage also influenced the central region, where stronger currents occurred on 2 September (~20 cms^{-1}, Fig. 12) and circulation over the eastern and central region is part of an overall cyclonic pattern (Fig. 17b). By contrast, before the HK passage on 1 September, the respective distribution revealed weaker winds (<6 m s^{-1}) and currents (<10 cm s^{-1}) over the central region, where the eastern boundary of the plume is extended. We deduce that strong currents forced by the hurricane winds also contributed to the decrease in *CI* values. The area of low *CIs* remains extensive 2 days after the passage of the HK eye away from the region (5 September), forming upper ocean conditions favorable to mixing and cooling before the following hurricane (HM) on 8 September 2011. The *Noriver* simulation shows low *CI* levels during the entire HK pre-storm and storm periods (Fig. 18d), which we attribute to the absence of Amazon-Orinoco plume waters and associated BL (very high SSS; Fig. 18b). Thus, the contribution of the hurricane forcing on wind-driven currents appears to be a secondary factor in the *CI* decrease, while its contribution on the salinity mixing that destroyed the river induced BL appears to be the dominant factor. The *CI* was a good indicator of ocean feedback to the evolution of the three successive hurricanes.

5 Conclusions

The interaction between the Amazon-Orinoco plume and three major hurricanes over the Atlantic Ocean is investigated with the high-resolution ATL-HYCOM 0.04° model during the 2011 hurricane season. The potential upper ocean contribution to the fate and intensification of the three hurricanes is examined by simulating the upper ocean dynamics and the evolution of the river plume characteristics under hurricane conditions. In general, results from numerical simulations showed good agreement with respective satellite and in situ observations over the Amazon-Orinoco study region, affected by passing hurricanes. The model computed low and peak temperature values similar to observations in summer–fall 2011. It exhibited some periods of overestimated SSS, which can lead to an underestimation of the effects of the BL. However, BL was generally represented well enough to allow the study of processes related to its variability. The unique combination of three successive major hurricanes over the plume region during a single month allowed us to study the impacts of different upper ocean and hurricane characteristics for each case, leading to different magnitude, size, and fate for each hurricane. HK was intensified over the plume region in early-September, while the two following tropical cyclones (TCs), HM, and HO, were weakened during their interaction with the plume-affected region (South West Atlantic Hurricane domain, AHSW; Fig. 1). These two TCs (HM and HO) were the only ones among all major hurricanes of 2009–2014 period, which did not intensify over the plume region. Our results lead to the conclusion that the upper ocean structure and evolution can contribute to hurricane intensity, in tandem with the impact of several atmospheric conditions, such as translation speed and humidity levels.

The upper ocean stratification of the AHSW region is strongly related to the northward spreading of the Amazon-

Orinoco plume, influencing the air-sea interaction during the TC propagation. The area of low-salinity waters over the AHSW was significantly reduced during all hurricane passages. However, the largest reduction took place during HK, indicating the beginning of the upper ocean mixing period. The upwelling of deep ocean waters is strongly related to the mixing induced by HK, which determined the stratification and formed different vertical structure conditions before the arrival of HM and HO. High levels of buoyancy frequency were present when HK entered the AHSW region, in agreement with the temperature and salinity vertical distributions. The halocline, induced by the Amazon-Orinoco plume, forms a strong pycnocline, resulting in a BL between the mixed layer and subsurface waters. The HK and HM passages over the study area further reduced the BLT. The BLT shrinkage allowed the mixing of the upper ocean with colder waters below and thus the increasing of both ILD and mixed layer depth. The smaller BL (~10 m), which prevailed after HK, allowed the cooling of the surface layers under HM and HO impacts and the formation of a stronger cold wake, inhibiting their intensification.

The evolution of several ocean metrics, related to the upper ocean thermal potential, showed that the HK passage over the region played a significant role on the storm intensification and increase in size. The existence of a BL kept the upper ocean warmer and favorable to hurricane intensification. However, the strong mixing induced after the HK and especially during the HM and HO periods reduced the potential energy that hurricanes were able to draw from the upper ocean layers. The *CI* index was also computed in order to measure the potential energy required to cool the ocean surface through mixing, by taking into account both thermal and haline stratification. The reduction of the BL due to river plume waters after the passage of HK was associated with low *CI* levels and thus weak resistance of the upper ocean to mixing caused by the hurricanes. The 2-day passage of HK over the plume-affected region reduced the ocean's resistance to mixing and formed upper ocean conditions more favorable to mixing and cooling. The contribution of the hurricane forcing on wind-driven currents appears to be a secondary factor in the *CI* decrease, while its contribution on the salinity mixing that destroyed the river induced BL appears to be the dominant factor. The *CI* levels in the case of plume absence (*Noriver* experiment) were significantly low, showing lower resistance of the upper ocean to mixing and cooling (lower stratification frequency levels).

Our results demonstrated numerical high-resolution ocean simulations over the broader Atlantic hurricane region that provided both the appropriate domain coverage and details in ocean dynamics (e.g., river plume evolution) to allow the study of processes associated with hurricane interaction with the upper ocean. Future coupled ocean-atmospheric model simulations (beyond the scope of this study) will provide additional details about the dynamics and evolution of the hurricanes over the North Atlantic. Given the ability to reproduce upper ocean conditions and describe targeted air-sea interaction processes, such as the influence of river plume dominated ocean regions on hurricane evolution, the free-running ATL-HYCOM simulation is effective to be used as the Nature Run model in the framework of an OSSE system over the Atlantic hurricane region.

Acknowledgments This study was funded by NOAA-OAR through a Sandy Supplemental award (NA13OAR4830224). V. Kourafalou received additional NOAA-OAR support (NA15OAR4320064). Internal support of G. Halliwell, M. Le Hénaff, and M. Mehari by NOAA-AOML-PhOD is gratefully acknowledged.

References

Androulidakis YS, Kourafalou VH (2013) On the processes that influence the transport and fate of Mississippi waters under flooding outflow conditions. Ocean Dyn 63(2–3):143–164

Androulidakis YS, Kourafalou VH, Krestenitis YN, Zervakis V (2012) Variability of deep water mass characteristics in the North Aegean Sea: the role of lateral inputs and atmospheric conditions. Deep-Sea Res I Oceanogr Res Pap 67:55–72

Balaguru K, Chang P, Saravanan R, Leung LR, Xu Z, Li M, Hsieh JS (2012a) Ocean barrier layers' effect on tropical cyclone intensification. Proc Natl Acad Sci 109(36):14343–14347

Balaguru K, Chang P, Saravanan R, Jang CJ (2012b) The Barrier Layer of the Atlantic warm pool: formation mechanism and influence on the mean climate. Tellus A 64

Balaguru K, Taraphdar S, Leung LR, Foltz GR, Knaff JA (2014) Cyclone-cyclone interactions through the ocean pathway. Geophys Res Lett 41(19):6855–6862

Banks CJ, Gommenginger CP, Srokosz M, Snaith HM (2012) Validating SMOS ocean surface salinity in the Atlantic with Argo and operational ocean model data. Geoscience and Remote Sensing, IEEE Transactions on 50(5):1688–1702

Barron CN, Smedstad LF (2002) Global River Inflow within the Navy Coastal Ocean Model. Proceedings, MTS/IEEE Oceans 2002 Conference, 1472–1479

Blake ES, Landsea C, Gibney EJ (2007) The deadliest, costliest, and most intense United States tropical cyclones from 1851 to 2006 (and other frequently requested hurricane facts) (p. 43). NOAA/National Weather Service, National Centers for Environmental Prediction, National Hurricane Center

Bleck R (2002) An oceanic general circulation model framed in hybrid isopycnic-Cartesian coordinates. Ocean Model 4(1):55–88

Bleck R, Halliwell G, Wallcraft A, Carrol S, Kelly K, Rushing K, (2002) Hybrid Coordinate Ocean Model (HYCOM). User's Manual, 199 pp

Brennan MJ (2012) Hurricane Maria Cyclone Report, National Hurricane Center, December 8, 2011. Available On Line: http://www.nhc.noaa.gov/data/tcr/AL142011_Maria.pdf

Cangialosi JP (2011) Hurricane Ophelia Tropical Cyclone Report, National Hurricane Center, December 8, 2011. Available On Line: http://www.nhc.noaa.gov/data/tcr/AL162011_Ophelia.pdf

Chassignet EP, Hurlburt HE, Smedstad OM, Halliwell GR, Hogan PJ, Wallcraft AJ, Bleck R (2007) The HYCOM (hybrid coordinate ocean model) data assimilative system. J Mar Syst 65(1):60–83

Coles VJ, Brooks MT, Hopkins J, Stukel MR, Yager PL, Hood RR (2013) The pathways and properties of the Amazon River plume in the

tropical North Atlantic Ocean. Journal of Geophysical Research: Oceans 118(12):6894–6913

Cummings JA, Smedstad OM (2013) Variational data assimilation for the global ocean. In: Data assimilation for atmospheric, oceanic and hydrologic applications (Vol. II). Springer Berlin Heidelberg, p 303–343

De Boyer Montégut C, Madec G, Fischer AS, Lazar A, Iudicone D (2004) Mixed layer depth over the global ocean: an examination of profile data and a profile-based climatology. Journal of Geophysical Research: Oceans 109(C12). doi:10.1029/2004JC002378

De Boyer Montégut C, Mignot J, Lazar A, Cravatte S, (2007) Control of salinity on the mixed layer depth in the world ocean: 1. General description. Journal of Geophysical Research: Oceans 112(C6). doi:10.1029/2006JC003953

Domingues R, Goni G, Bringas F, Lee S-K, Kim H-S, Halliwell G, Dong J, Morell J, Pomales L (2015) Upper Ocean response to hurricane Gonzalo (2014): salinity effects revealed by targeted and sustained underwater glider observations. Geophys Res Lett 42:7131–7138. doi:10.1002/2015GL065378

Donlon C, Casey K, Gentemann C, LeBorgne P, Robinson I, Reynolds R, Merchant C, Llewellyn-Jones D, Minnett P, JF P, Cornillon P (2009) Successes and challenges for the modern sea surface temperature observing system. Proceedings of the OceanObs 21:9

Emanuel KA (1987) The dependence of hurricane intensity on climate. Nature 326(6112):483–485

Felton CS, Subrahmanyam B, Murty VSN, Shriver JF (2014) Estimation of the barrier layer thickness in the Indian Ocean using Aquarius salinity. Journal of Geophysical Research: Oceans 119(7):4200–4213

Ffield A (2005) North Brazil current rings viewed by TRMM microwave imager SST and the influence of the Amazon plume. Deep Sea Res I 52(1):137–160

Ffield A (2007) Amazon and Orinoco River plumes and NBC rings: bystanders or participants in hurricane events? J Clim 20(2):316–333

Fisher EL (1958) Hurricanes and the sea-surface temperature field. J Meteorol 15(3):328–333

Forget G, Ferron B, Mercier H (2008) Combining Argo profiles with a general circulation model in the North Atlantic. Part 1: estimation of hydrographic and circulation anomalies from synthetic profiles, over a year. Ocean Model 20(1):1–16

Fratantoni DM, Johns WE, Townsend TL (1995) Rings of the North Brazil current: their structure and behaviour inferred from observations and a numerical simulation. J Geophys Res 100:10633–10654

Gierach MM, Vazquez-Cuervo J, Lee T, Tsontos VM (2013) Aquarius and SMOS detect effects of an extreme Mississippi River flooding event in the Gulf of Mexico. Geophys Res Lett 40(19):5188–5193

Goldenberg SB, Landsea CW, Mestas-Nuñez AM, Gray WM (2001) The recent increase in Atlantic hurricane activity: causes and implications. Science 293(5529):474–479

Goni G, Johns WE (2001) A census of North Brazil current rings observed from TOPEX/POSEIDON altimetry: 1992-1998. Geophys Res Lett 28(1):1–4

Goni G, Black P, Trinanes J (2003) Using satellite altimetry to identify regions of hurricane intensification. Aviso. Newsletter 9:19–20

Gray WM (1979) Hurricanes: their formation, structure and likely role in the tropical circulation. Meteorology over the tropical oceans 77: 155–218

Grodsky SA, Reul N, Lagerloef G, Reverdin G, Carton JA, Chapron B, Quilfen Y, Kudryavtsev VN, Kao HY (2012) Haline hurricane wake in the Amazon/Orinoco plume: AQUARIUS/SACD and SMOS observations. Geophysical Research Letters 39(20). doi:10.1029/2012GL053335.

Grodsky SA, Reverdin G, Carton JA, Coles VJ (2014) Year-to-year salinity changes in the Amazon plume: contrasting 2011 and 2012 Aquarius/SACD and SMOS satellite data. Remote Sens Environ 140:14–22

Guinehut S, Larnicol G, Le Traon PY (2002) Design of an array of profiling floats in the North Atlantic from model simulations. J Mar Syst 35(1):1–9

Halliwell GR (2004) Evaluation of vertical coordinate and vertical mixing algorithms in the HYbrid-Coordinate Ocean Model (HYCOM. Ocean Model 7(3):285–322

Halliwell GR, Srinivasan A, Kourafalou V, Yang H, Willey D, Le Hénaff M, Atlas R (2014) Rigorous evaluation of a fraternal twin ocean OSSE system for the open Gulf of Mexico. J Atmos Ocean Technol 31(1):105–130

Halliwell GR, Gopalakrishnan S, Marks F, Willey D (2015a) Idealized study of ocean impacts on tropical cyclone intensity forecasts. Mon Weather Rev 143:1142–1165

Halliwell GR, Kourafalou V, Le Hénaff M, Shay LK, Atlas R (2015b) OSSE impact analysis of airborne ocean surveys for improving upper ocean dynamical and thermodynamical forecasts in the Gulf of Mexico. Prog Oceanogr 130:32–46

Johns WE, Lee TN, Schott FA, Zantopp RJ, Evans RH (1990) The North Brazil Current retroflection: seasonal structure and eddy variability. Journal of Geophysical Research: Oceans 95(C12):22103–22120

Jullien S, Menkes CE, Marchesiello P, Jourdain NC, Lengaigne M, Koch-Larrouy A, Lefevre J, Vincent EM, Faure V (2012) Impact of tropical cyclones on the heat budget of the South Pacific Ocean. J Phys Oceanogr 42(11):1882–1906

Jullien S, Marchesiello P, Menkes CE, Lefèvre J, Jourdain NC, Samson G, Lengaigne M (2014) Ocean feedback to tropical cyclones: climatology and processes. Clim Dyn 43(9–10):2831–2854

Kendall MG (1975) Rank correlation methods, 4th edition. Charles Griffin, London

Kim HS, Vecchi GA, Knutson TR, Anderson WG, Delworth TL, Rosati A, Zeng F, Zhao M (2014) Tropical cyclone simulation and response to CO_2 doubling in the GFDL CM2. 5 high-resolution coupled climate model. J Clim 27(21):8034–8054

Kourafalou VH, Androulidakis YS (2013) Influence of Mississippi River induced circulation on the Deepwater horizon oil spill transport. Journal of Geophysical Research: Oceans 118(8):3823–3842

Kourafalou VH, Oey L-Y, Wang JD, Lee TN (1996) The fate of river discharge on the continental shelf. Part I: modeling the river plume and the inner-shelf coastal current. J Geophys Res 101(C2):3415–3434. doi:10.1029/95JC03024

Kourafalou VH, Androulidakis YS, Halliwell GR, Kang H, Mehari M, Le Hénaff M, Atlas R, Lumpkin R (2016) North Atlantic Ocean OSSE system development: nature run evaluation and application to hurricane interaction with the Gulf Stream. Prog Oceanogr 145:1–25

Lagerloef G (2012) Satellite mission monitors ocean surface salinity. Eos, Transactions American Geophysical Union 93(25):233–234

Lagerloef G, Colomb FR, Le Vine D, Wentz F, Yueh S, Ruf C, Lilly J, Gunn J, Chao Y, deCharon A, Feldman G (2008) The Aquarius/SAC-D mission: designed to meet the salinity remote-sensing challenge. Oceanography 21(1):68–81

Landsea CW, Gray WM (1992) The strong association between western Sahelian monsoon rainfall and intense Atlantic hurricanes. J Clim 5(5):435–453

Large WG, McWilliams JC, Doney SC (1994) Oceanic vertical mixing: a review and a model with a nonlocal boundary layer parameterization. Rev Geophys 32(4):363–404

Leipper DF, Volgenau D (1972) Hurricane heat potential of the Gulf of Mexico. J Phys Oceanogr 2(3):218–224

Lentz SJ (1995) Seasonal variations in the horizontal structure of the Amazon plume inferred from historical hydrographic data. Journal of Geophysical Research: Oceans (1978–2012) 100(C2):2391–2400

Lewis K, Allen JI (2009) Validation of a hydrodynamic-ecosystem model simulation with time-series data collected in the western English Channel. J Mar Syst 77(3):296–311

Liu Y, MacCready P, Hickey BM (2009) Columbia River plume patterns in summer 2004 as revealed by a hindcast coastal ocean circulation model. Geophys Res Lett 36(2). doi:10.1029/2008GL036447

Lukas R, Lindstrom E (1991) The mixed layer of the western equatorial Pacific Ocean. J Geophys Res 96:3343–3357

Mainelli M, DeMaria M, Shay LK, Goni G (2008) Application of oceanic heat content estimation to operational forecasting of recent Atlantic category 5 hurricanes. Weather Forecast 23(1):3–16

Mann HB (1945) Non-parametric tests against trend. Econometrica 13: 163–171

Masson S, Delecluse P (2001) Influence of the Amazon River runoff on the tropical Atlantic. Physics and Chemistry of the Earth, Part B: Hydrology, Oceans and Atmosphere 26(2):137–142

Merrill RT (1984) A comparison of large and small tropical cyclones. Mon Weather Rev 112(7):1408–1418

Muller-Karger FE, McClain CR, Richardson PL (1988) The dispersal of the Amazon's water. Nature 333(6168):56–59

Muller-Karger FE, Richardson PL, McGillicuddy D (1995) On the offshore dispersal of the Amazon's plume in the North Atlantic: comments on the paper by A. Longhurst, "Seasonal cooling and blooming in tropical oceans. Deep-Sea Res I Oceanogr Res Pap 42(11): 2127–2137

Neetu, S., Lengaigne, M., Vincent, E.M., Vialard, J., Madec, G., Samson, G., Ramesh Kumar MR, Durand F (2012) Influence of upper-ocean stratification on tropical cyclone-induced surface cooling in the Bay of Bengal. Journal of Geophysical Research: Oceans 117(C12). doi:10.1029/2012JC008433.

Newinger C, Toumi R (2015) Potential impact of the colored Amazon and Orinoco plume on tropical cyclone intensity. Journal of Geophysical Research: Oceans 120(2):1296–1317

Pailler K, Bourlès B, Gouriou Y (1999) The barrier layer in the western tropical Atlantic Ocean. Geophys Res Lett 26(14):2069–2072

Pearson K (1903) Mathematical contributions to the theory of evolution. XI. On the influence of natural selection on the variability and correlation of organs. Philos Trans R Soc Lond 200:1–66

Peng MS, Reynolds CA (2006) Sensitivity of tropical cyclone forecasts as revealed by singular vectors. J Atmos Sci 63(10):2508–2528

Price JF (1981) Upper Ocean response to a hurricane. J Phys Oceanogr 11(2):153–175

Price JF (2009) Metrics of hurricane-ocean interaction: vertically-integrated or vertically-averaged ocean temperature? Ocean Sci 5: 351–368

Reul N, Fournier S, Boutin J, Hernandez O, Maes C, Chapron B, Alory G, Quilfen Y, Tenerelli J, Morisset S, Kerr Y (2014a) Sea surface salinity observations from space with the SMOS satellite: a new means to monitor the marine branch of the water cycle. Surv Geophys 35(3):681–722

Reul N, Quilfen Y, Chapron B, Fournier S, Kudryavtsev V, Sabia R (2014b) Multisensor observations of the Amazon-Orinoco river plume interactions with hurricanes. Journal of Geophysical Research: Oceans 119(12):8271–8295

Samson G, Giordani H, Caniaux G, Roux F (2009) Numerical investigation of an oceanic resonant regime induced by hurricane winds. Ocean Dyn 59(4):565–586

Sanford TB, Price JF, Girton JB (2011) Upper-ocean response to hurricane Frances (2004) observed by profiling EM-APEX floats. J Phys Oceanogr 41(6):1041–1056

Schade LR, Emanuel KA (1999) The ocean's effect on the intensity of tropical cyclones: results from a simple coupled atmosphere-ocean model. J Atmos Sci 56(4):642–651

Schiller RV, Kourafalou VH (2010) Modeling river plume dynamics with the HYbrid Coordinate Ocean Model. Ocean Model 33(1):101–117

Schiller RV, Kourafalou VH, Hogan P, Walker ND (2011) The dynamics of the Mississippi River plume: Impact of topography, wind and offshore forcing on the fate of plume waters. Journal of Geophysical Research: Oceans (1978–2012) 116(C6)

Sengupta D, Goddalehundi BR, Anitha DS (2008) Cyclone-induced mixing does not cool SST in the post-monsoon North Bay of Bengal. Atmos Sci Lett 9(1):1–6

Shay LK, Black PG, Mariano AJ, Hawkins JD, Elsberry RL (1992) Upper Ocean response to Hurricane Gilbert. J Geophys Res 97(20):227–220

Shay LK, Mariano AJ, Jacob SD, Ryan EH (1998) Mean and near-inertial ocean current response to Hurricane Gilbert. J Phys Oceanogr 28(5): 858–889

Shay LK, Goni GJ, Black PG (2000) Effects of a warm oceanic feature on Hurricane Opal. Mon Weather Rev 128(5):1366–1383

Sprintall J, Tomczak M (1992) Evidence of the barrier layer in the surface layer of the tropics. J Geophys Res 97(C5):7305–7316

Steel RG, James H (1960) Principles and procedures of statistics: with special reference to the biological sciences. McGraw-Hill, New York, 519.5, S314

Stewart SR (2012) Hurricane Katia Tropical Cyclone Report. National Hurricane Center, December 8, 2011. Available On Line: http://www.nhc.noaa.gov/data/tcr/AL122011_Katia.pdf

Vincent EM, Lengaigne M, Vialard J, Madec G, Jourdain NC, Masson S (2012) Assessing the oceanic control on the amplitude of sea surface cooling induced by tropical cyclones. Journal of Geophysical Research: Oceans (1978–2012) 117(C5). doi:10.1029/2011JC007705.

Vizy EK, Cook KH (2010) Influence of the Amazon/Orinoco Plume on the summertime Atlantic climate. Journal of Geophysical Research: Atmospheres (1984 2012), 115(D21)

Wang C, Liu H, Lee SK, Atlas R (2011) Impact of the Atlantic warm pool on United States landfalling hurricanes. Geophysical Research Letters 38(19). doi:10.1029/2011GL049265.

Willmott CJ (1981) On the validation of models. Phys Geogr 2(2):184–194

Wu L (2007) Impact of Saharan air layer on hurricane peak intensity. Geophysical Research Letters 34(9). doi:10.1029/2007GL029564.

Zamudio L, Hogan PJ (2008) Nesting the Gulf of Mexico in Atlantic HYCOM: oceanographic processes generated by Hurricane Ivan. Ocean Model 21(3):106–125